ARTICLES
https://doi.org/10.1038/s44161-022-00064-2

nature cardiovascular research

Syndecan-2 selectively regulates VEGF-induced vascular permeability

F. Corti[1], E. Ristori[1], F. Rivera-Molina[2], D. Toomre[2], J. Zhang[1], J. Mihailovic[3], Z. W. Zhuang[1] and M. Simons[1]✉

Vascular endothelial growth factor (VEGF)-driven increase in vascular permeability is a key feature of many disease states associated with inflammation and ischemic injury, contributing significantly to morbidity and mortality in these settings. Despite its importance, no specific regulators that preferentially control a VEGF-dependent increase in permeability versus its other biological activities have been identified. Here, we report that a proteoglycan, Syndecan-2 (Sdc2), regulates the interaction between a transmembrane phosphatase, DEP1, and VEGFR2 by controlling cell surface levels of DEP1. In the absence of Sdc2 or the presence of an antibody that blocks the Sdc2–DEP1 interaction, increased plasma membrane DEP1 levels promote selective dephosphorylation of the VEGFR2 Y951 site that is involved in permeability control. Either an endothelial-specific Sdc2 deletion or a treatment with an anti-Sdc2 antibody results in a marked reduction in stroke size due to a decrease in intracerebral edema.

Dynamic control of vascular permeability is central to homeostasis maintenance. Although under normal conditions, most vascular beds do not allow free movement of solute and cells, this can rapidly change in response to both physiological and pathological stimuli[1–3]. VEGF is one of the most potent inducers of permeability. VEGF levels increase dramatically in settings of acute ischemic injury or chronic inflammation due to the presence of inflammatory cells capable of producing the growth factor, with a strong contribution of inflammation-induced edema attributable to VEGF activity[4–7]. VEGF exerts its permeability-inducing effects by binding to its principal signaling receptor, VEGFR2, leading to phosphorylation of tyrosine Y951 (human equivalent of mouse Y949) and activation of the Src cascade[8–11]. The latter event promotes disassembly of adherens and tight junctions with the resultant increase in vascular leakiness[12–16].

VEGF belongs to a family of heparin-binding growth factors, and its interactions with VEGFR2 are governed by the presence of heparan sulfate (HS) chains carrying proteoglycans on the cell surface[17,18]. One of these proteoglycans, the transmembrane protein Sdc2 has been recently shown to carry HS chains that preferentially bind $VEGFA_{165}$ (ref. [19]). To gain understanding of the role of Sdc2 in VEGF biology, we undertook a study of its function in regulation of vascular permeability.

We first examined the effect of Sdc2 knockout on VEGF signaling responses in primary mouse endothelial cells (ECs). As expected, there was a mild reduction in phosphorylation of the VEGFR2 Y1175 kinase site (Y1173 in mouse) that was previously traced to a reduction in $VEGFA_{165}$-VEGFR2 binding in the absence of Sdc2 HS chains[19] (Fig. 1a,b). Because HS chains facilitate VEGFR2 occupation by $VEGFA_{165}$, we expected other VEGFR2 phosphosites to be equally affected in Sdc2 null ($Sdc2^{-/-}$) ECs. However, although there was a comparable decline in VEGFR2 Y1059 (Y1057 in mouse) phosphorylation (~25% decrease for Y1059 and Y1175 at 5 min post-$VEGFA_{165}$ stimulation) (Fig. 1a,c), there was a larger reduction of Y951 (~40% decrease at 5 min post-$VEGFA_{165}$ stimulation) (Fig. 1a,d) suggesting that Sdc2 may regulate VEGFR2 activation in phosphotyrosine-specific manner. To test whether Sdc2 core protein could be play a role in such mechanism, we measured VEGFR2 activation following treatment with non-HS-binding $VEGFA_{121}$[20]. In contrast to $VEGFA_{165}$ stimulation, there was no statistically significant reduction in either Y1059 or Y1175 phosphorylation (Fig. 1f–h). However, there was a 40% reduction in Y951 phosphorylation (Fig. 1f,i) that was similar in magnitude to that seen with $VEGFA_{165}$. Src activation is the major downstream event following VEGFR2 Y951 phosphorylation[9]. Accordingly, we found that VEGFA-induced Src activation was impaired in $Sdc2^{-/-}$ ECs in response to both $VEGFA_{165}$ and $VEGFA_{121}$ (Fig. 1a,e and Fig. 1f,j). Sdc2 knockdown in human umbilical vein ECs (HUVECs) confirmed decreased Y951 phosphorylation and reduced Src activation following $VEGFA_{165}$ and $VEGFA_{121}$ stimulation (Extended Data Fig. 1a,b)

Phosphorylation of VEGFR2 Y951 site is known to activate the Tsad–Src–vascular endothelial (VE)-cadherin pathway, which controls junctional stability and permeability[21]. To test whether Sdc2 knockout affects the permeability response, we used the Miles assay[22]. Mice with a global Sdc2 deletion ($Sdc2^{-/-}$), endothelial-specific deletion of Sdc2 (obtained by crossing $Cdh5CreR^{T2}$ line[23] with $Sdc2^{fl/fl}$, hereby referred to as $Sdc2^{iECKO}$) or wild-type (WT) controls were injected intradermally with $VEGFA_{165}$, $VEGFA_{121}$ or histamine, and the extent of vascular permeability in the skin was measured by Evans blue dye extravasation. Both VEGFs induced a much smaller extent of dye extravasation in $Sdc2^{-/-}$ (Fig. 1k–n) and $Sdc2^{iECKO}$ mice (Extended Data Fig. 1c) compared to WT control mice. At the same time, Sdc2 knockout had no effect on the vascular permeability response to histamine (Fig. 1o,p). We also assessed baseline vascular integrity of $Sdc2^{-/-}$ mice by measuring Evans blue extravasation in various organs in the absence of VEGF stimulation. In all cases, basal permeability in these mice was comparable to WT controls (Extended Data Fig. 1d).

To investigate the molecular basis of reduced Y951 phosphorylation and a corresponding reduction in VEGF-induced permeability in $Sdc2^{-/-}$ and $Sdc2^{iECKO}$ mice, we studied expression of key members

[1]Yale Cardiovascular Research Center Department of Internal Medicine, Yale University School of Medicine, New Haven, CT, USA. [2]Department of Cell Biology, Yale University School of Medicine, New Haven, CT, USA. [3]Department of Radiology and Biomedical Imaging, Yale University School of Medicine, New Haven, CT, USA. ✉e-mail: michael.simons@yale.edu

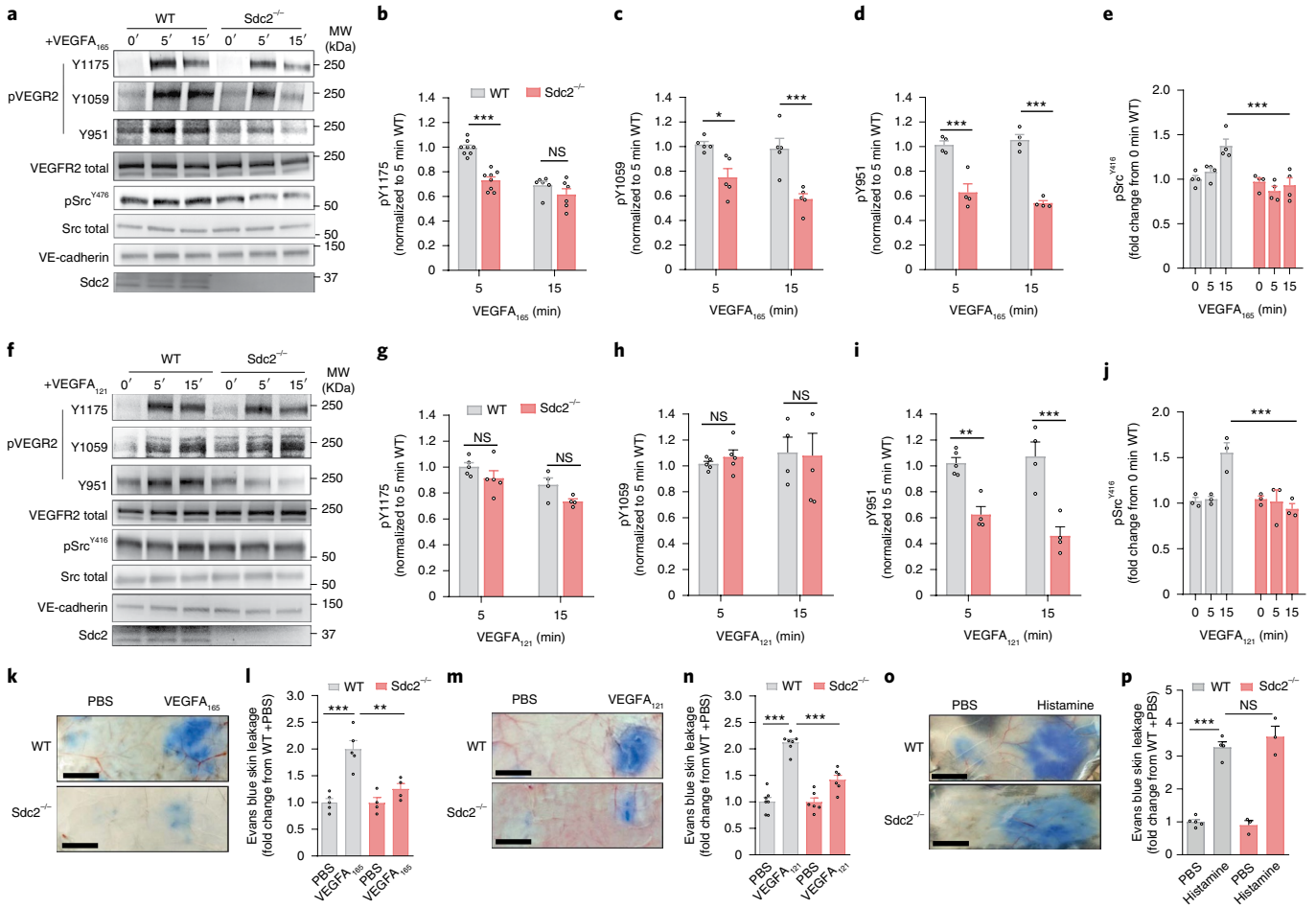

Fig. 1 | Sdc2 deletion leads to reduced VEGFA-induced Y951 phosphorylation and permeability in vivo. a–e, Western blot analysis and quantification of VEGFR2 phosphorylation (pVEGFR2) and Src activation ($pSrc^{Y416}$) in WT versus Sdc2$^{-/-}$ mouse ECs after 5–15 minutes (min) of stimulation with $VEGFA_{165}$ (50 ng ml^{-1}) versus PBS (phosphate-buffered saline) vehicle ($n=4$–8). MV, molecular weight. **f–j**, western blot analysis and quantification of VEGFR2 phosphorylation and Src activation ($pSrc^{Y416}$) in WT versus Sdc2$^{-/-}$ mouse ECs 5–15 min of stimulation with $VEGFA_{121}$ (50 ng ml^{-1}) ($n=4$–5). **k,l**, $VEGFA_{165}$-induced Evans blue dye leakage in the back skin (Miles assay) of WT versus Sdc2$^{-/-}$ mice (scale bars, 500 µm) ($n=4$–5). **m,n**, $VEGFA_{121}$-induced Evans blue dye leakage in the back skin of WT versus Sdc2$^{-/-}$ mice (scale bars, 500 µm) ($n=6$–7). **o,p**, Histamine-induced Evans blue dye leakage in the back skin of WT versus Sdc2$^{-/-}$ mice (scale bars, 500 µm) ($n=3$–5). Data are presented as mean values ± s.e.m. (standard error of the mean), and each dot represents a biological independent experiment (n). Statistical analysis was performed by two-way analysis of variance (ANOVA) with Sidak's multiple comparison test (b–e,g–j) or one-way ANOVA with Sidak's multiple comparison test (l,n,p) (NS, not significant; $^{*}P<0.05$; $^{**}P<0.01$; $^{***}P<0.001$).

of VEGF signaling cascade and its regulators, including membrane receptor phosphatases VEPTP (ref. [24]) and DEP1 (refs. [25,26]), and the intracellular ER-anchored PTP1B (ref. [27]). Sdc2 knockout had no effect on total cellular levels of VEGF receptors (VEGFR1, VEGFR2 and Neuropilin-1 (Nrp1)), the adhesion protein VE-cadherin and the three phosphatases (Fig. 2a). However, examination of the cell surface levels of these proteins demonstrated a significant increase in DEP1 levels in Sdc2$^{-/-}$ ECs (Fig. 2b,c). An increased DEP1 surface level was confirmed in HUVECs following Sdc2 knockdown (Extended Data Fig. 1e,f).

To check whether this increase in cell surface DEP1 could account for a selective increase in VEGFR2 Y951 dephosphorylation, we transduced HUVECs with an adenovirus carrying the DEP1 expression construct. Overexpression of DEP1 reduced $VEGFA_{165}$-induced Y951 but had minimal effect on Y1059 or Y1175 sites phosphorylation (Fig. 2d–f).

To show that this effect is DEP1 specific, we performed a knockdown of the three phosphatases known to affect VEGFR2 signaling[28] and measured their impact on the extent of $VEGFA_{165}$-induced VEGFR2 phosphorylation. In agreement with published studies[29], PTP1b knockdown preferentially increased Y1175 phosphorylation, leaving the Y951 site phosphorylation unchanged (Fig. 2g,j), whereas VEPTP knockdown increased phosphorylation of all examined VEGFR2 sites (Fig. 2h,j). In contrast, DEP1 knockdown preferentially increased Y951 phosphorylation, whereas phosphorylation levels of Y1059 and Y1175 were minimally affected (Fig. 2i,j).

DEP1 is a transmembrane phosphatase enriched at cell–cell contacts in ECs and other cell types[30,31], which interacts with various components of the adherens junction complex (e.g., VE-cadherin, p120-catenin and β-catenin)[32]. Indeed, we observed that DEP1 was mostly localized at cell junctions of confluent ECs (Extended Data Fig. 2a). Both Sdc2 and DEP1 are expressed at the cell surface (Extended Data Fig. 2b) and can engage in a direct interaction[33], whereas Sdc2 HS chains mediate formation of a ternary complex with $VEGFA_{165}$ and VEGFR2 following $VEGFA_{165}$ stimulation in ECs. Therefore, we hypothesized that DEP1 surface level are linked to endocytosis of the $VEGFA_{165}$–VEGFR2–Sdc2 ternary complex as it gets internalized in tandem with Sdc2. The absence of Sdc2 would reduce DEP1 cell entry, thereby increasing its plasma membrane

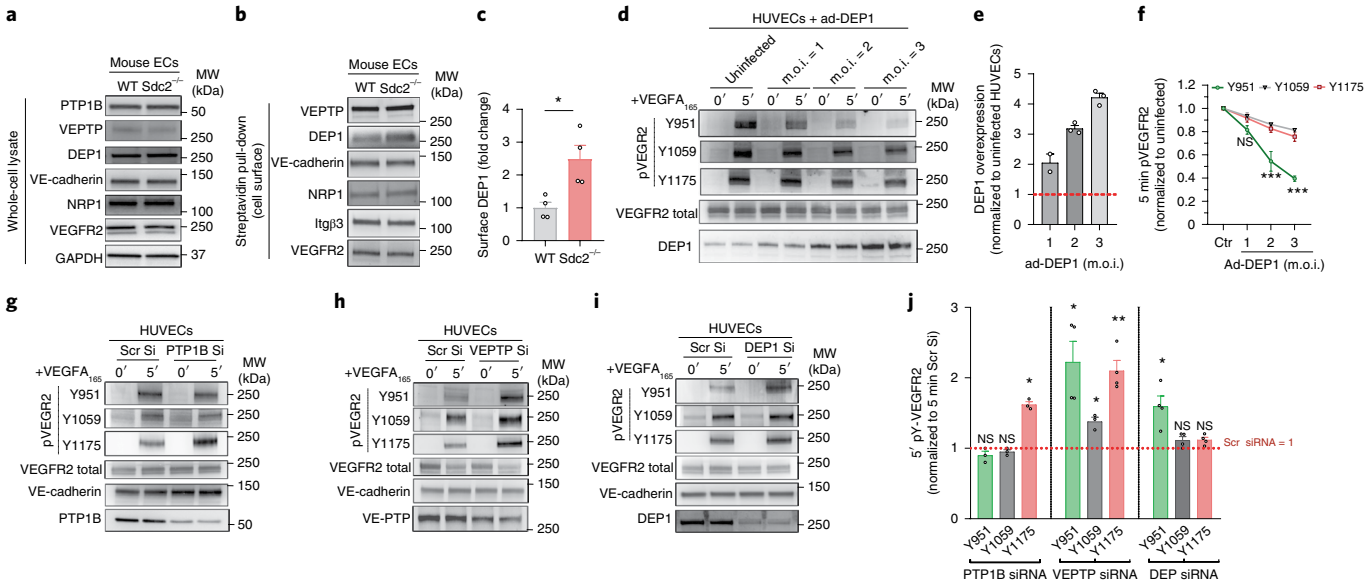

Fig. 2 | Increased DEP1 surface level in Sdc2$^{-/-}$ mouse ECs promotes selective dephosphorylation of VEGFR2 Y951 (Y951 in mouse). a, Western blot analysis of protein levels in whole-cell lysates of WT vs Sdc2$^{-/-}$ mouse ECs (representative blot of three independent experiments). **b**, Western blot analysis of cell membrane protein levels by streptavidin pull-down (cell surface) in WT versus Sdc2$^{-/-}$ mouse ECs. **c**, Quantification of DEP1 levels at the cytoplasmic membrane (surface) ($n=4$). **d**–**f**, Assessment of VEGFA$_{165}$-induced VEGFR2 phosphorylation (pVEGFR2) after DEP1 overexpression in HUVECs ($n=3$–4). Red line (e) represents endogenous DEP1 levels normalized to 1. **g**–**j**, Assessment of VEGFA$_{165}$-induced VEGFR2 phosphorylation after silencing of PTP1B with siRNA (Si) (PTP1B Si), VEPTP (VEPTP Si) and DEP1 (DEP1 Si) in HUVECs ($n=3$–4). Data are presented as mean values ± s.e.m. In all figure panels, each dot represents a biological independent experiment (n). Statistical analysis was performed by unpaired two-tailed Student's t-test (c) or two-way ANOVA with Sidak's multiple comparison test (e,f,j) (*$P<0.05$; **$P<0.01$; ***$P<0.001$). m.o.i., multiplicity of infection; siRNA, short interfering RNA.

levels and decreasing VEGFR2 Y951 site phosphorylation, thereby reducing permeability.

To test this possibility, we first evaluated whether Sdc2 and Dep1 internalize with a time course similar to VEGFR2. VEGFA$_{165}$ stimulation in HUVECs led to a prompt internalization of all three proteins with a similar kinetics, as shown by decreasing cell surface levels (Fig. 3a,b). Furthermore, structural illumination microscopy (SIM) analysis showed that VEGFA$_{165}$ stimulation led to a higher colocalization of Sdc2 (Fig. 3c) and DEP1 (Fig. 3d) with VEGFR2 in Rab5$^+$ endosomes, indicating that Sdc2 and DEP1 internalization follows a clathrin-mediated endocytic process like VEGFR2 (ref. [29,34]). SIM images also revealed copresence of Sdc2/DEP1 in Rab5$^+$ and VEGFR2$^+$ endosomal structures (Extended Data Fig. 2c–f), suggesting a molecular link among Sdc2, DEP1 and VEGFR2.

To assess whether Sdc2 is required for DEP1 internalization, we isolated primary ECs from WT and Sdc2$^{-/-}$ mice and measured DEP1 internalization after VEGFA$_{165}$ stimulation. We observed that DEP1, but not VEGFR2, internalization was greatly impaired in the absence of Sdc2 (Fig. 3e–h). We then used immunofluorescence to examine DEP1 and VEGFR2 internalization in response to VEGF stimulation in WT and Sdc2$^{-/-}$ primary ECs transduced with comparable levels of surface HA-tagged DEP1. The loss of Sdc2 led to a decrease of internalized DEP1 that colocalized in VEGFR2$^+$ endocytic complexes (Fig. 3i,j).

We also examined whether DEP1 undergoes constitutive endocytosis in the absence of added VEGFA$_{165}$ and whether it is dependent on Sdc2. HUVECs kept in the VEGFA-free media displayed a degree of constitutive DEP1 internalization, which was reduced after Sdc2 knockdown (Extended Data Fig. 2g,h). Moreover, confocal images of HUVECs showed the presence of DEP1–Sdc2 complexes in Rab5$^+$ endosomal compartments in the absence of VEGFA stimulation (Extended Data Fig. 2i).

Overall, these results suggest that a Sdc2–DEP1 interaction is necessary for DEP1 internalization. To formally prove this hypothesis, we generated a polyclonal antibody against DEP1-binding domain of Sdc2[33] mouse sequence (Extended Data Fig. 3a) in an attempt to disrupt Sdc2–DEP1 association. Validation of this anti-Sdc2 polyclonal antibody (Sdc2 pAb) confirmed specific binding to Sdc2, but not Syndecan-4 (Sdc4) (Extended Data Fig. 3b). Furthermore, HUVECs transduced with mouse Sdc2 (V5-tag) and human DEP1 (HA-tag) constructs followed by treatment with the Sdc2 pAb showed a marked reduction in Sdc2–DEP1 association (Fig. 3k).

We then tested the ability of the Sdc2 pAb to block VEGFA$_{165}$-induced DEP1 internalization in mouse brain ECs (bEnd.3 cells). Preincubation of bEnd.3 cells with Sdc2 pAb (1 hr) prevented VEGFA$_{165}$-induced DEP1 internalization compared to IgG treatment (Fig. 3l,m,o). In agreement with decreased Y951-Src activation, internalization of VE-cadherin was also reduced upon treatment with Sdc2 pAb (Fig. 3l,m). However, VEGFR2 internalization was not affected by treatment with Sdc2 pAb (Fig. 3l–n). In line with these findings, Sdc2 pAb preferentially led to decreased phosphorylation of VEGFR2 Y951 versus Y1175 (Fig. 3p,q). Finally, to evaluate the functional consequence of the Sdc2 pAb treatment, we studied the effect of this pAb treatment on bEnd.3 cells in vitro. In agreement with a strong decrease in Y951 activation, cells treated with the Sdc2 pAb showed inhibition of VEGFA-induced decline in trans-endothelial electrical resistance (Fig. 3r), a measure of endothelial barrier integrity that normally correlates with changes in vascular permeability in vivo[35]. In contrast, VEGFA$_{165}$-induced proliferation and migration were not affected by Sdc2 pAb treatment (Extended Data Fig. 3c–e)

VEGFA-induced permeability plays a pathogenic role in a number of disease processes[36,37]. In particular, a rapid rise in VEGFA$_{165}$ levels following a stroke is thought to destabilize the blood–brain barrier, leading to a peri-infarct edema (vasogenic edema) and unregulated entrance into the brain parenchyma of blood-borne substances that further increase the damage, leading to a substantial

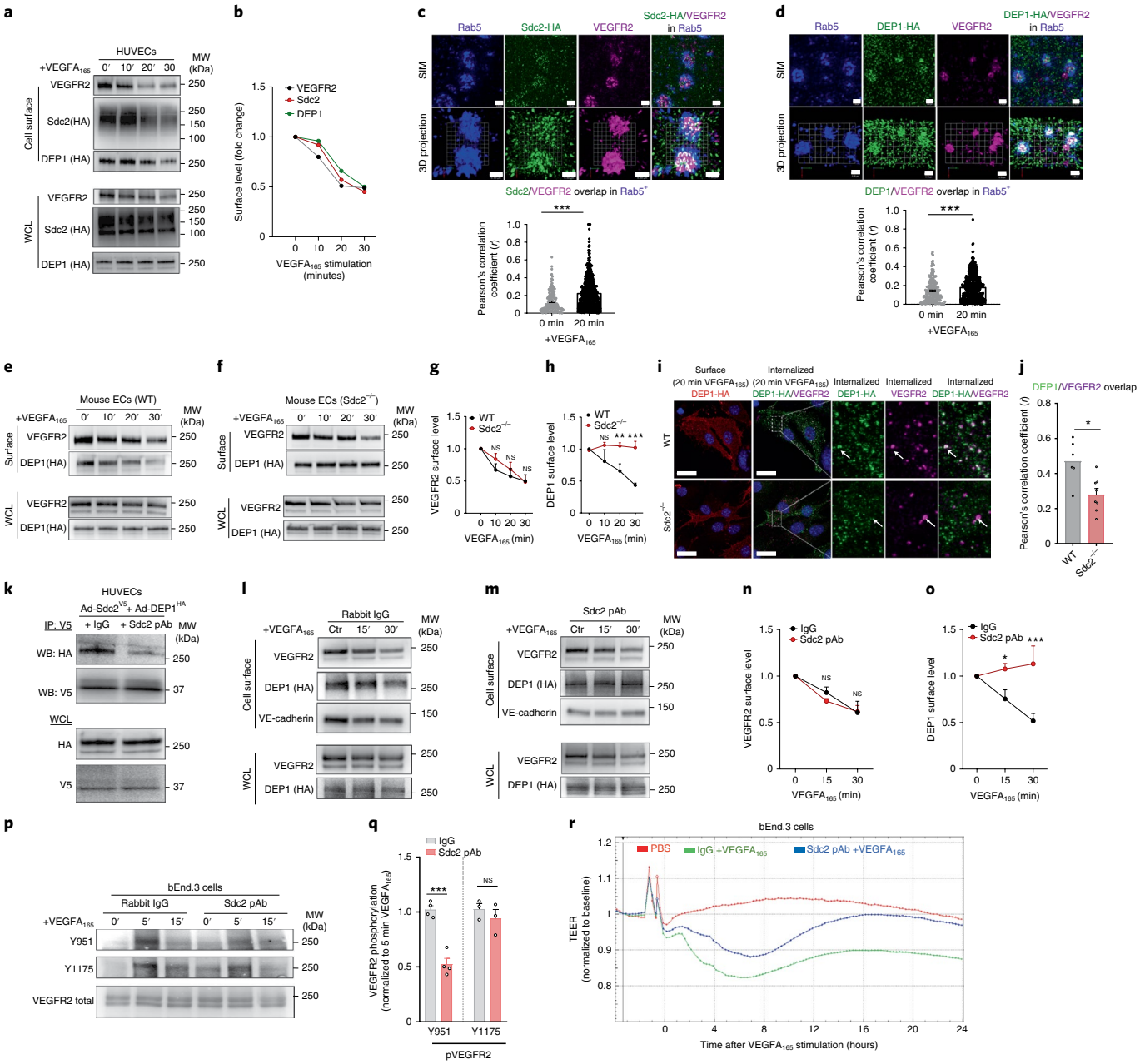

Fig. 3 | Sdc2–DEP1 interaction regulates DEP1 surface level and can be exploited to achieve specific inhibition of VEGFA-induced permeability. **a**,**b**, Western blot analysis and quantification of cell surface protein levels after $VEGFA_{165}$ (100 ng ml^{-1}) stimulation in HUVECs. For increased sensitivity, the experiment was performed in HUVECs after overexpression of either Sdc2 or DEP1 carrying N-terminal HA-tag. **c**,**d**, SIM imaging of endosomal Sdc2–VEGFR2 and DEP1–VEGFR2 complexes in HUVECs expressing human Sdc2 or DEP1 carrying N-terminal HA-tag (Sdc2-HA and DEP1-HA) and treated for 20 min with 50 ng ml^{-1} $VEGFA_{165}$. Scale bars, 0.5 µm. Quantification shows the levels of colocalization of Sdc2or DEP1 and VEGFR2 in Rab5+ objects. Each point indicates a Rab5^{+} endosome. **e–h**, Western blot analysis and quantification of cell surface protein levels following $VEGFA_{165}$ (100 ng ml^{-1}) in WT vs Sdc2$^{-/-}$ mouse ECs. ($n = 3 = 5$). **i**, confocal imaging of primary mouse WT and Sdc2$^{-/-}$ ECs infected with adenovirus expressing human DEP1 carrying N-terminal HA-tag (DEP1-HA) protein and treated for 20 min with 50 ng ml^{-1} VEGFA165. In red, the superficial expression of DEP1 shows comparable infection levels of WT and Sdc2$^{-/-}$ sample. The colocalization of internalized DEP1-HA (green) and internalized VEGFR2 (purple) was reduced in Sdc2$^{-/-}$ ECs (white arrows). Scale bars, 25 µm. **k**, Sdc2/DEP1 Co-Ip in presence of rabbit immunoglobulin G (+IgG) or an antibody against DEP-binding motif in Sdc2 (Sdc2 pAb) (representative blot of three independent experiments). **l–o**, Western blot analysis of cell surface protein levels following $VEGFA_{165}$ (100 ng ml^{-1}) stimulation in bEnd.3 cells. Cells were preincubated for 1 hr with a rabbit IgG (5 µg ml^{-1}) or the Sdc2 pAb (5 µg ml^{-1}) before $VEGFA_{165}$ stimulation ($n = 3 = 4$). **p**,**q**, assessment of VEGFA-induced VEGFR2 phosphorylation after preincubation (1.5 h) with a rabbit IgG (5 µg ml^{-1}) or Sdc2 pAb (5 µg ml^{-1}). **r**, In vitro permeability response in bEnd.3 cells in response to $VEGFA_{165}$ (100 ng ml^{-1}) in the presence of a rabbit IgG (5 µg ml^{-1}) or Sdc2 pAb (5 µg ml^{-1}) ($n = 3$–4). Data are presented as mean values ± s.e.m. In all figure panels, each dot represents a biological independent experiment (n). Statistical analysis was performed by two-way ANOVA with Sidak's multiple comparison test (g,h,n,o) or one-way ANOVA with Sidak's multiple comparison (q) (*$P < 0.05$; **$P < 0.01$; ***$P < 0.001$). IP, immunoprecipitation; WB, western blot; WCL, whole-cell lysates.

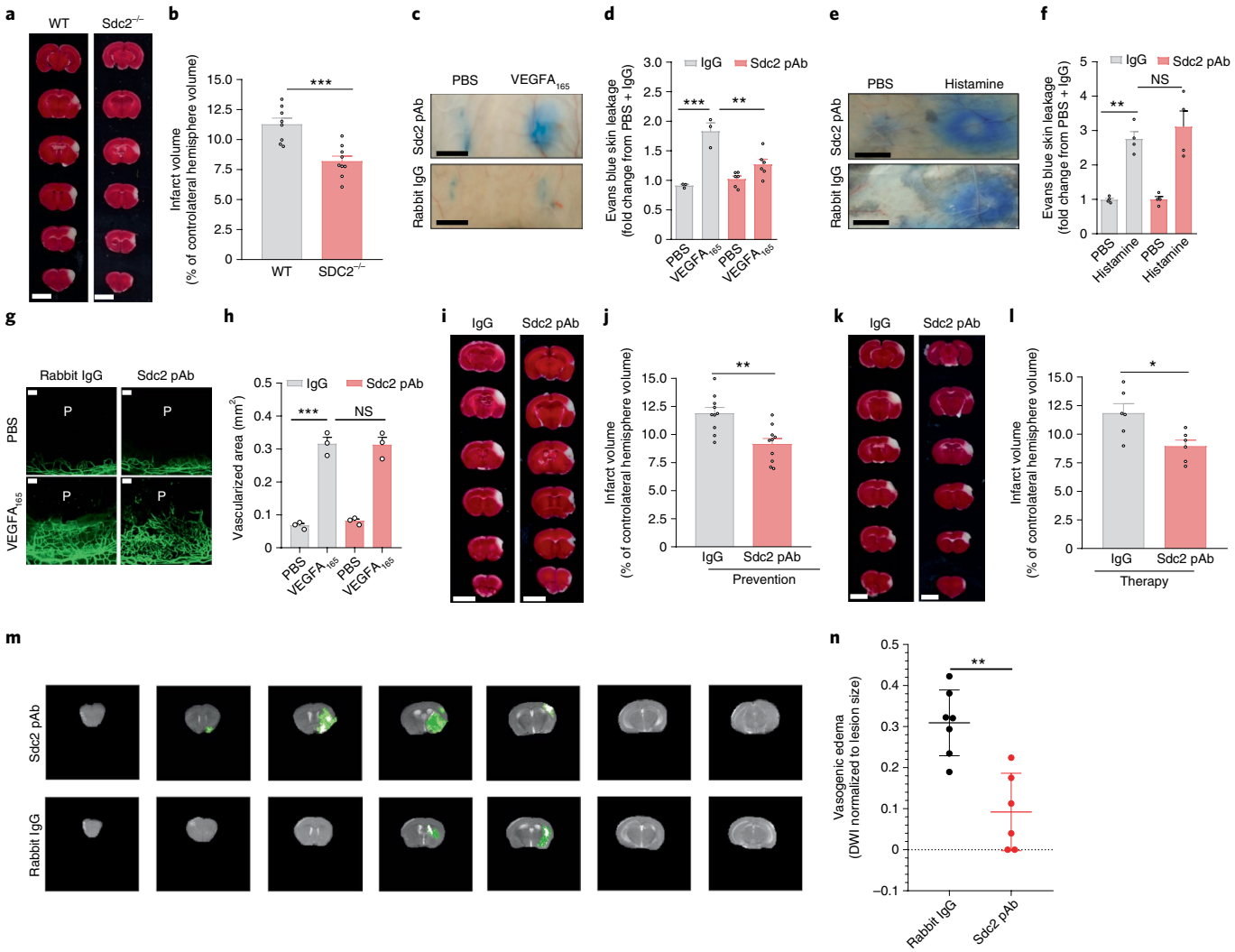

Fig. 4 | Sdc2 deletion or treatment with an antibody that blocks the Sdc2–DEP1 interaction confers neuroprotection in a mouse focal stroke model. **a,b**, TTC staining (24 h stroke) and quantification of stroke infarct in WT versus Sdc2$^{-/-}$ mice ($n = 8$–9). **c,d**, $VEGFA_{165}$-induced Evans blue dye leakage in the back skin of mice treated with rabbit IgG or Sdc2 pAb (intravenous (i.v.) injection of the antibody was performed 1.5 h before $VEGFA_{165}$ stimulation) ($n = 3$–6). **e,f**, Histamine-induced Evans blue leakage in the back skin of mice treated with rabbit IgG or Sdc2 pAb (i.v. injection of the antibody was done 1.5 h before $VEGFA_{165}$ stimulation) ($n = 4$). **g,h**, Cornea pocket angiogenesis assay in mice treated with rabbit IgG or Sdc2 pAb (scale bars, 100 µm). The position of $VEGFA_{165}$ pellet (P) is labeled in each cornea image. **i–l**, TTC staining at 24 h and quantification of stroke size in mice treated with rabbit IgG or Sdc2 pAb before (prevention, i,j) ($n = 6$) or 1 hr after (therapy, k,l) ($n = 10$) stroke induction. **m,n**, MRI compartmentalization analysis (Methods) allowed separation of the ischemic stroke core (white), penumbra (light green) and edema (dark green) and quantification of vasogenic edema normalized to total stroke size ($n = 6$–7). Data are presented as mean values ± s.e.m. In all figure panels, each dot represents a biological independent experiment (n). Statistical analysis was performed by unpaired two-tailed Student's t-test (b,j,l,n) or one-way ANOVA with Sidak's multiple comparison test (d,f,h) (*$P < 0.05$; **$P < 0.01$; ***$P < 0.001$). DWI, diffusion-weighted imaging.

increase in the final infarct size[38–40]. Because Sdc2$^{-/-}$ mice display a reduced permeability in response to VEGFA, we set out to test whether this translates into reduced stroke size in these mice. To this end, we induced an acute stroke in Sdc2$^{-/-}$ and WT mice with a permanent ligation of the distal middle cerebral artery (MCA) via craniectomy[41]. Morphometric evaluation of the infarct size 24 h after ligation using TTC (2,3,5-triphenyltetrazolium chloride) live staining demonstrated a significant 35% reduction in the stroke size (Fig. 4a,b). To assess whether reduced infarct size is due Sdc2 deletion in ECs, we repeated the same stroke model in Sdc2^{iECKO} mice (Extended Data Fig. 3f,g). Here, we observed a reduction in infarct size similar to that observed in global Sdc2$^{-/-}$ mice, suggesting that reduced endothelial permeability is the main driver of the neuroprotective effect of Sdc2 deletion.

Finally, we set out to evaluate the therapeutic potential of preventing VEGF-induced edema formation by blocking the Sdc2–DEP1 interaction with our validated antibody described above (Sdc2 pAb). First, we checked the effectiveness of the Sdc2 pAb in modulating skin permeability. An i.v. injection of the blocking Sdc2 pAb antibody abolished VEGFA-induced permeability in the mouse skin mice compared to IgG controls (Fig. 4c,d) However, Sdc2 pAb did not affect the skin permeability response to histamine (Fig. 4e,f) or inhibit $VEGFA_{165}$-induced angiogenesis in a cornea pocket assay (Fig. 4g,h).

We then tested whether the Sdc2 blocking antibody could confer neuroprotection in the same mouse stroke model as used in Sdc2 null mice. Indeed, i.v. injection either before (Fig. 4i,j) or after MCA ligation (Fig. 4k,l) resulted in significant reduction in the infarct size

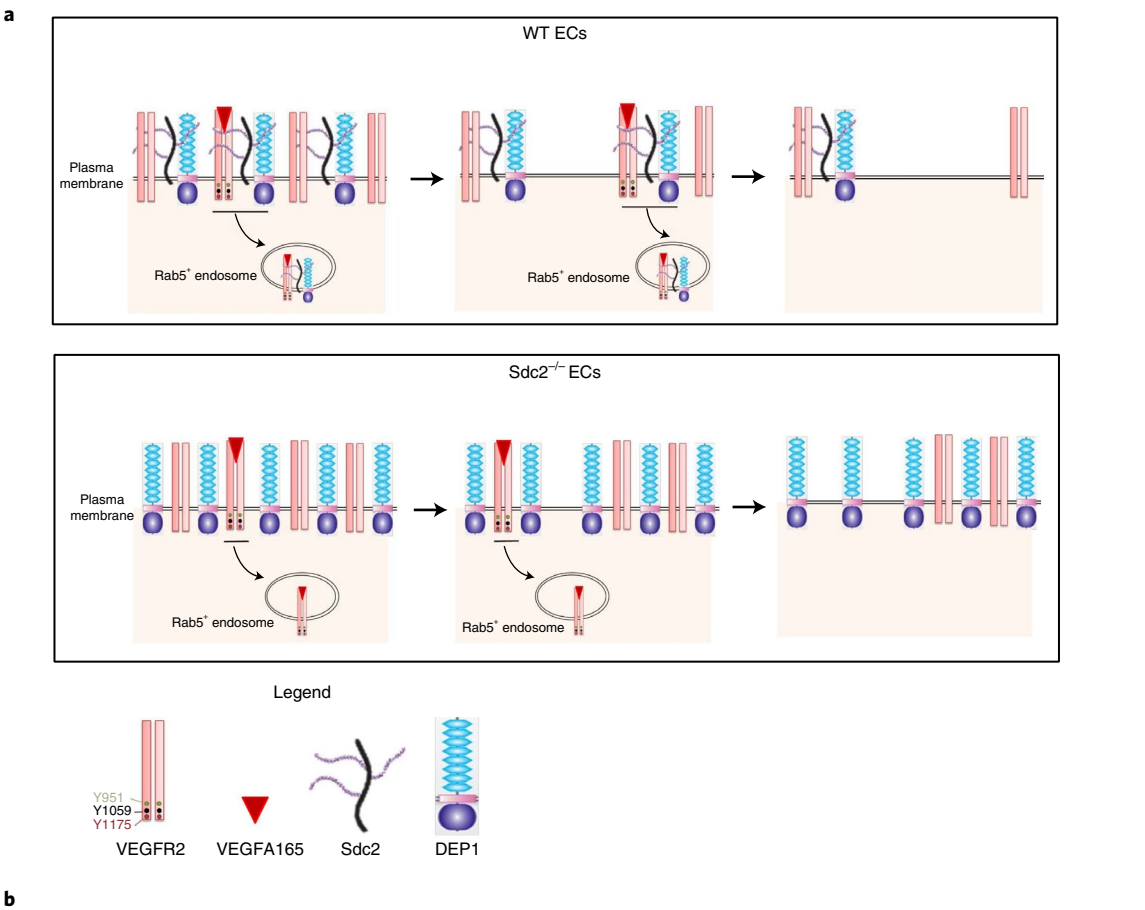

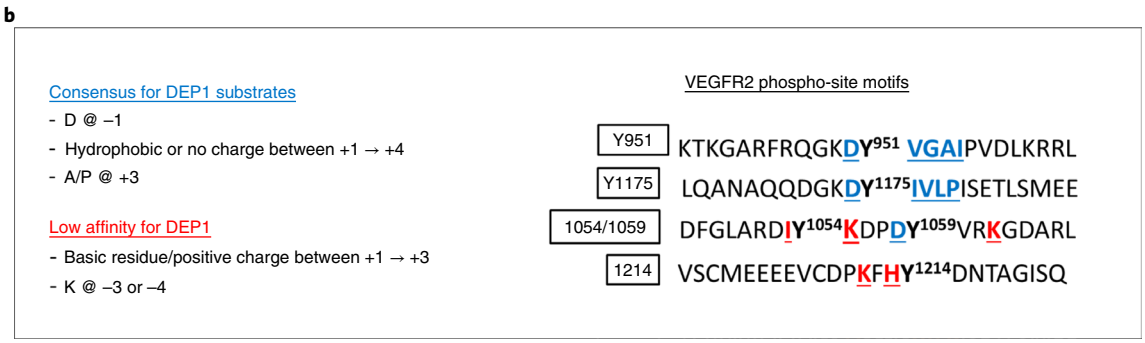

Fig. 5 | Proposed working model for regulation of DEP1 surface level by Sdc2. a, Proposed working model for accumulation of DEP1 at the cell surface and specific VEGFR2 Y951 dephosphorylation. The key control point is Sdc2-dependent endocytosis of DEP1. The two proteins normally exist in a heteromeric complex on the EC surface, with Sdc2 internalization triggering DEP1 endocytosis and thereby reducing its ability to dephosphorylate the VEGFR2 Y951 site at the cell surface (top). In the absence of Sdc2, DEP1's inability to internalize leads to an increased stochiometric ratio of DEP1/VEGFR2 at the cell surface (bottom), selective dephosphorylation of the VEGFR2 Y951 site and reduction in permeability response. **b**, DEP1 selectivity toward different phosphotyrosine residues is influenced by the surrounding amino acids. Criteria were extrapolated from multiple studies assessing DEP1 target preferences[58–60]. Aspartic acid at the −1 position (D @ −1) is associated with increased tyrosine dephosphorylation by DEP1. Conversely, a lysine residue at the −3 or −4 position (K @ −3 or −4) seems to inhibit DEP1 dephosphorylation. Additional criteria are reported in figure panel **b**.

after 24hrs. Finally, we found that treatment of Sdc2 null mice with Sdc2 pAb did not alter stroke size (Extended Data Fig. 3h,i), indicating antibody specificity towards Sdc2 function.

To further confirm that the neuroprotective effect was due to Sdc2 pAb's ability to inhibit vasogenic edema, we used multimodal magnetic resonance imaging (MRI) to quantify the volume of the edema in IgG- and Sdc2 pAb-treated mice. To this end, we performed a transient occlusion of the MCA (45-min occlusion followed by reperfusion) and then injected either the Sdc2 pAb or a control IgG 30 min after reperfusion. Brain MRI scanning was then performed 24 h later. Compartmentalization analysis of MRI images (Extended Data Fig. 4 and Methods show mathematical details) allowed us to define affected areas as the ischemic stroke core (white), penumbra (light green) and extracellular vasogenic edema (dark green) (Fig. 4m). Quantification of these parameters revealed that mice receiving Sdc2 pAb developed markedly less vasogenic edema compared to IgG-treated mice, indicating that Sdc2 pAb treatment has an anti-edematous effect in ischemic stroke (Fig. 4n)

Discussion

These results describe a pathway selectively regulating VEGF-induced vascular permeability. The key control point is Sdc2-dependent endocytosis of DEP1 (Fig. 5). The two proteins normally exist in a heteromeric complex on the EC surface, with

Sdc2 internalization triggering DEP1 endocytosis and thereby reducing its ability to dephosphorylate the VEGFR2 Y951 site at the cell surface. In the absence of Sdc2, DEP1's inability to internalize leads to an increased stochiometric ratio of DEP1/VEGFR2 at the cell surface, selective dephosphorylation of the VEGFR2 Y951 site and reduction in permeability response. The surprising specificity of DEP1 for Y951 may be due to the amino acid sequence flanking the site that closely resembles the DEP1 consensus binding site (Fig. 5b).

Interestingly, we observed a more selective defect of Y951 phosphorylation with $VEGFA_{121}$ stimulation compared to $VEGFA_{165}$, likely because $VEGFA_{165}$, but not $VEGFA_{121}$, requires Sdc2 HS chains to efficiently occupy VEGFR2 (ref. [19]). Consequently, $VEGFA_{165}$-induced, but not $VEGFA_{121}$-induced, VEGFR2 phosphorylation in Sdc2 null ECs is somewhat reduced globally (~25%) in other phosphotyrosine sites. At the same time, $VEGFA_{121}$- induced VEGFR2 phosphorylation, which is HS independent, is reduced only on the Y951 site, further demonstrating a direct causal relationship between plasma membrane levels of DEP1 and VEGFR2 Y951 phosphorylation. In agreement with such explanation, we found that increasing DEP1 surface level through overexpression led to a selective decrease in VEGFR2 Y951 phosphorylation in response to $VEGFA_{165}$ stimulation (Fig. 2d).

In addition, VEGFR2 Y951 phosphorylation in Sdc2 null ECs appears to decrease even below baseline following stimulation with VEGFA. Baseline VEGFR2 phosphorylation can be the consequence of ligand-independent activation mechanisms such the effect of fluid shear stress[42] and direct Src activity toward VEGFR2 tyrosine sites[43]. Thus, one possible explanation for a Y951 decrease below baseline after VEGFA stimulation is that once VEGFR2 starts to internalize, it is displaced from transactivation mechanisms. Another possibility is simply that once VEGFR2 gets inside the cells, it is exposed to intracellular phosphatases[28] that further decrease Y951 phosphorylation below baseline.

Mechanistically, Sdc2 forms a heteromeric complex with DEP1, likely due to a direct binding of the latter to Sdc2 (ref. [33]). $VEGFA_{165}$ binding to Sdc2 HS chains brings Sdc2, along with its DEP1 partner, into the $VEGFA_{165}$–VEGFR2 complex. VEGFA-triggered internalization of VEGFR2 pulls Sdc2 and its DEP1 partner along. In the absence of Sdc2, DEP1 is not internalized with the VEGFA–VEGFR2 complex, resulting its accumulation on the plasma membrane and increased VEGFR2 Y951 dephosphorylation.

Sdc2, as all other Syndecans, can undergo shedding on the cell surface[44], and its shed extracellular domain can interact with DEP1 (ref. [33]). In this study, we have not specifically investigated whether Sdc2 shedding is involved in regulation of permeability, and we cannot exclude a possibility that this process may also play a role in modulation of DEP1 surface levels and VEGFR2 dephosphorylation. A recent study reported that Sdc4 can induce activation and internalization of VE-cadherin[45]. How Sdc4 does that and whether this modulation is involved in a specific regulation of VEGFA-induced permeability is not clear. Because Sdc2 and Sdc4 can form an heterodimer[46], it is also possible that Sdc4 can modulate Sdc2 distribution at the cell membrane.

Importantly, the Sdc2–DEP1 interaction can be exploited for therapeutic purposes; an antibody blocking this protein–protein interaction leads to an increase in cell surface DEP1 levels and a decreased permeability response to VEGFA. In functional terms, this was effective as the Sdc2 knockout, resulting in a important reduction in stroke size. The Sdc2 polyclonal antibody we employed (Sdc2 pAb) disrupts the Sdc2–DEP1 interaction by targeting the DEP1-binding motif on the Sdc2 core protein. This does not affect $VEGFA_{165}$ binding to Sdc2 HS chains, which are required for full VEGFR2 activation and angiogenesis. As a result, the only impaired VEGFR2 signaling pathway is VEGFR2–Y951-dependent phosphorylation activation of Src signaling and vascular permeability[3,10], with minimal interference with other VEGFA biological effects. In agreement with these findings, a selective inactivation of a Y951-Src pathway in a mouse genetic model (VEGFR2 Y951F mutation) results in live mice without angiogenic defects but with a specific impairment of VEGFA-induced vascular permeability[21].

No changes in basal permeability were seen in Sdc2 null mice in this study, implying that the DEP1–VEGFR2 interaction does not regulate this process. On the other hand, conditions that lead with increased endothelial Sdc2 expression such as inflammation and hypoxia[47–49] may also increase basal permeability, as Sdc2 HS chains can sensitize VEGFR2 activation[19]. Thus, increasing the level of Sdc2 HS chains might ultimately lead to enough VEGFR2 activation to alter vascular permeability even under physiological $VEGFA_{165}$ concentrations.

Finally, DEP1 has been shown to modulate endothelial barrier function by dephosphorylation of various proteins of adherens and tight junctions (e.g., VE-cadherin, p120 catenin, γ-catenin β-catenin, occludin)[32]. Thus, we cannot exclude that a direct effect of higher surface DEP1 on junction proteins may contribute to the observed permeability phenotype in Sdc2 null mice due to one of these interactions. Additionally, if the absence of Sdc2 results in changes in junctional phosphorylation, then it is possible that other biological process such as leukocyte transmigration and shear stress sensing may also be affected in Sdc2 null mice.

In summary, Sdc2 is a regulator of a VEGF-dependent vascular permeability response that acts by controlling cell surface DEP1 levels, thereby enabling a selective regulation of a specific VEGF signaling pathway. This unique feature of Sdc2-dependent regulation of permeability makes it an appealing therapeutic target for treatment of conditions such as stroke[39,40], where suppression of permeability needs to be coupled with preservation of the vasculature and VEGFA neuroprotective and neurogenic effects[36,50,51].

Methods

List of antibodies and growth factors. The following is a list of antibodies with applications and dilutions: pVEGFR2 Y1175 (WB 1:1,000, Cell Signaling, 2478), pVEGFR2 Y1059 (for HUVECs, western blot (WB) 1:1,000, Cell Signaling Technology, 3817), pVEGFR2 Y1059 (for mouse ECs, WB 1:1,000, EMD Millipore, ABS553), pVEGFR2 Y951 (WB 1:1,000, Cell Signaling Technology, 4991), VEGFR2 total (WB 1:1,000, Cell Signaling Technology, 2479), VE-cadherin (for HUVECs, WB 1:200, Santa Cruz Biotechnology, sc-9989 (F-8)), VE-cadherin (for mouse ECs, WB 1:500, BD Pharmingen, 555289), mouse Sdc2 (WB 1:200, R&D Systems, AF6585 - polyclonal raised against mouse Sdc2 extracellular domain), human Sdc2 (WB 1:200, R&D Systems, AF2965, polyclonal raised against human extracellular domain), mouse PTP1b (WB 1:200, Santa Cruz Biotechnology, sc-1718-R (N19-R)), human PTP1b (WB 1:500, BD Pharmingen, 610139), VEPTP (VE-PTP-C pAb69 and VE-PTP 1-8 pAb70 were gifts from D. Vestweber, Max Plank Institute for Molecular Biomedicine), DEP1 (WB 1:200, Santa Cruz Biotechnology, sc-21761 (143-41)), NRP1 (WB 1:1,000, Cell Signaling Technology, 3725,), HA-tag (WB 1:1,000, Cell Signaling Technology, 3724), rabbit anti-Rab5 (Cell Signaling Technology, 3547, immunohistochemistry (IHC) 1:200), goat anti-VEGFR2 (R&D Systems, AF357, IHC 1:100), mouse anti-HA.11 (Covance, MMS-101P, IHC 1:200), rabbit anti-HA (Cell Signaling Technology, 3724, IHC 1:200), rabbit anti-VE-cadherin (Cell Signaling Technology, 2500, IHC 1:200), goat anti-mouse VE-cadherin (R&D Systems, AF1002, IHC 1:100) and rat anti-mouse Flk1 (BD Pharmingen, 555307, IHC 1:100).

Growth factors used were $VEGFA_{165}$ (R&D Systems, 293-VE-010) and $VEGFA_{121}$ (R&D Systems, 4644-VS-010).

Animal studies. All mouse experimental protocols have been approved by the Institutional Animal Care & Use Committee at Yale University. The authors have complied with all relevant animal testing and research ethical regulations. All transgenic mice used in this study have been previously described[19], including Sdc2 knockout-first transgenic mice (Sdc2tm1a(KOMP)Wtsi), Sdc2 null mice ($Sdc2^{-/-}$), Sdc2 conditional transgenic mice ($Sdc2^{fl/fl}$) and Sdc2 endothelial-specific knockout ($sdc2^{icdh5}$). All animals were back-crossed at least ten generations to a C57Black6/J strain. For this study, male mice (*mus musculus)* between the ages of 9–15 weeks were used .

Detection of Syndecan expression by western blotting. For Sdc2 detection in mouse ECs and HUVECs, heparinase pretreatment is required to unveil epitopes on core protein and remove nonspecific sugar epitopes. Briefly, confluent ECs on

6-cm tissue culture dishes were rinsed twice with DPBS. Cells were then incubated with 1.5 ml serum-free media (Thermo Fisher Scientific, Opti-MEMr) containing 2 U Heparinase I-III (Sigma-Aldrich, H2519 and H8891) and 1 U Heparinase II (Sigma-Aldrich, H6512). After 2.5-h digestion at 37 °C under gentle agitation, cells were washed three times with ice-cold PBS and lysed in 250 µl RIPA buffer. Samples were then analyzed by western blot. Specific Sdc2 core protein bands can be observed at ~37 kDa and ~48 kDa. Additional specific band smears, due to Sdc2 glycosylation isoforms (50–250 kDa), can sometimes be observed if heparinase digestion of HS chains is incomplete.

For HA-tag syndecans, heparinase pretreatment is not required. HA detection revealed naked core proteins in a dimeric form and additional higher-molecular-weight smear bands due to glycosylation isoforms.

Cell culture and mouse EC isolation. HUVECs were obtained from the Yale VBT tissue culture core laboratory at passage 1 and maintained in complete EGM-2 MV medium (Lonza). HUVECs were used for experiments between postnatal days 2 and 6. Primary mouse ECs were isolated as previously described[52]. Briefly, four hearts or lungs were harvested, finely minced with scissors and digested (37 °C for 45 min under gentle agitation) with 25 ml 1.5 mg ml^{-1} Collagenase/Dispase solution for heart (Sigma-Aldrich, 10269638001) or 2 mg ml^{-1} collagenase type I (Sigma-Aldrich, C0130). The crude preparation was triturated passing it ten times through a cannula needle, filtered on a 70-µM sterile cell strainer, and spun at 400 *g* for 10 min. Pellet was resuspended in 2 ml 0.1% BSA and 50 µl magnetic Dynabeads (Thermo Fisher Scientific, 11035) precoated overnight with anti-mouse CD31 (BD Pharmingen, 553370) added for EC positive selection. Selection was carried out for 25 min at room temperature under slow rotation. The bead-bound cells were recovered with a magnetic separator and washed five times with DMEM containing 10% FBS. Cells were finally resuspended in 10 ml complete DMEM medium (20% FBS with endothelial growth factor supplement (ECGS) and antibiotics) and seeded onto gelatin-precoated 10-cm plates. The bEnd.3 cell line was purchased from ATCC (CRL-2299) and maintained in DMEM with 10% FBS and streptomycin/penicillin. The bEnd.3 cell line was purchased from ATCC (CRL-2299), whereas 293 A cells were purchased from Invitrogen (R70507).

Cloning and adenovirus production. Adenoviruses expressing various syndecan sequences were generated as previously reported[52]. Briefly, presynthesized blunt-end sequences corresponding to Sdc2 or DEP1 constructs (IDT) were subcloned into a pENTR/D-TOPO (Invitrogen) vector, and then transferred via LR recombination into a pAD/CMV/V5-DEST adenoviral vector (Invitrogen). Adenoviruses were generated by transfection of this plasmid into HEK293 A (Invitrogen) after PACI linearization.

Growth factor stimulation and western blot analysis. HUVECs or mouse ECs were seeded onto 6-cm plates in a complete medium. Confluent cells were serum-starved in Opti-MEM media (Thermo Fisher Scientific, 31985070) for 6–8 h and then stimulated with the indicated agent. Cells were rapidly washed twice with ice-cold PBS and lysed with 200 µl RIPA lysis buffer containing protease/phosphatase inhibitor cocktail. Total lysates were cleared with a 16,000 *g* spin, and protein concentration was determined using the BCA method. Samples were added with reducing loading buffer, boiled for 5 min and loaded on 4–15% gels for SDS-PAGE separation. Proteins were then transferred to polyvinylidene difluoride Immobilon-P membranes (Millipore), blocked for 1 h in 5% fat-dry milk TBS-T (0.05% Tween) followed by 4 °C overnight incubation the primary antibody. Protein bands were visualized using horseradish peroxidase-conjugated secondary antibodies associated with enhanced chemiluminescence (Immobilon Western, Millipore). Signal from chemiluminescence reaction was recorded in a digital acquisition system (G-Box by Syngene) equipped with a charge-coupled device camera. Linear range is automatically calculated by the software and is displayed as a histogram with each acquired image. Images without band saturation were used for densitometric quantification. Total intensity of each band was determined with ImageJ software[53]. Molecular weights on western blot images are reported in kilodaltons.

Gene silencing in HUVECs. HUVECs were seeded onto 6-well plates and transfected at 80% confluency with 2.5 ml Opti-MEM (Thermo Fisher Scientific) with indicated siRNA plus 2.5 µl Lipofectamine RNA iMAX (Thermo Fisher Scientific) for 6–8 h. Transfection mix was replaced with full media (EGM-2 MV) for 48 h, then cell starved in 2% FBS for 6–8 h before growth factor stimulation. The following siRNAs were used for knockdown experiments in HUVECs: Sdc2 (Origene, SR321721 – C, 40 nM), VEPTP (Sigma-Aldrich SASI_Hs02_00324728, 60 nM), PTP1B Sigma-Aldrich SAS1_Hs01_00230699, 60 nM) and DEP1 (Qiagen, SI0265877 HS_PTPRJ_6, 60 nM).

Analysis of cell surface protein level by biotinylation. For evaluation of total surface protein level, confluent HUVECs or mouse ECs (10-cm dish) were transferred to an ice bed, washed three times with cold DPBS and then treated with 5 ml of a solution cell-impermeable biotinylation reagent (EZ-Link Sulfo-NHS-LC-Biotin, Thermo Fisher Scientific, 21335, 0.25 mg ml^{-1} in PBS with calcium/magnesium) for 1 h at 4 °C under gentle agitation. Cells were then placed back on ice, washed three times with 50 mM Tris in DPBS (pH = 7.4) and lysed with 1.6 ml RIPA buffer. Samples were spun at 16,000 *g* for 10 min, and 1.3 ml cleared lysate (~600 µg) was used for pull-down with neutravidin agarose beads (Thermo Fisher Scientific, 29202, 50 µl per sample) for 2 h at 4 °C under rotation. Beads were then washed four times with 1.5 ml RIPA lysis buffer, resuspended in 90 µl 2× sample buffer and boiled for 7 min.

For surface internalization experiments, cells were transduced with indicated adenovirus (m.o.i. ~2) for 16 h, serum-starved in Opti-MEM for 8 h, stimulated with $VEGFA_{165}$ (100 ng ml^{-1}) for the indicated times followed by surface biotinylation and neutravidin pull-down as described above.

Coimmunoprecipitation. Confluent HUVECs (10-cm dish) were transduced for 24 h in complete media (EGM-2 MV) with an adenovirus expressing mouse Sdc2 (V5-tag, m.o.i. ~6). Cells were split 1:3, allowed to grow for 3 more days and then transduced again with DEP1 (HA-tag, MOI~2) for 24 h. Before immunoprecipitation, cells were incubated for 1.5 h with rabbit IgG (5 µg ml^{-1}) or Sdc2 pAb (5 µg ml^{-1}) and then washed twice with ice-cold PBS, lysed in 1.6 ml in 1% Triton lysis buffer and spun at 16,000 *g* for 10 min; 600 µg (~1.3 ml) cleared lysate was then immunoprecipitated with 50 µl per sample of preabsorbed anti-V5 magnetic beads (Chromotek, v5tma; beads were preabsorbed with 1.6 ml of HUVEC cell lysate for 1 h at 4 °C) for 1 h at 4 °C under gentle rotation. Magnetic beads were washed three times with 1.5 ml Triton lysis buffer, resuspended in 80 µl 1× sample buffer and boiled for 5 min.

Immunocytochemistry. Because we were unable to obtain an effective antibody against DEP1 and Syndecan-2 (SDC2) for immunocytochemistry, we infected HUVECs for 48 h with adenovirus expressing N-terminal HA-tagged human DEP1 to visualize DEP1 cellular localization, and N-terminal HA-tagged or SNAP-tagged human SDC2 to visualize Sdc2. After the indicated treatment cells were processed for immunocytochemistry. Briefly, cells were first washed with PBS, fixed in 4% PFA for 10 min, and permeabilized by incubation in 2% PFA, 0.1% Triton-X, 0.1% NP-40 for an additional 10 min. Blocking was performed by incubation in 3% BSA (in PBS) for 1 h at room temperature. Cells were then incubated overnight at 4 °C in 1% BSA (in PBS) containing appropriate primary antibodies. The following primary antibodies were used: rabbit anti-Rab5 (Cell Signaling Technology, 3547 1:200); goat anti-VEGFR2 (R&D Systems, AF357, 1:100); mouse anti-HA.11 (Covance, MMS-101P, 1:200); rabbit anti-HA (Cell Signaling Technology, 3724, 1:200); rabbit anti-VE-cadherin (Cell Signaling Technology, 2500, 1:200); goat anti-mouse VE-cadherin (R&D Systems, AF1002, 1:100); rat anti-mouse Flk1 (BD Pharmingen, 555307, 1:100). On the following day, cells were washed with PBS and incubated in 1% BSA (in PBS) containing appropriate Alexa Flour-conjugated secondary antibodies used at a dilution of 1:400 for 1 h at room temperature. Cell nuclei were counterstained with DAPI (Thermo Fisher Scientific, 62248, 1:1,000) for 5 min at room temperature. After washing in PBS, cells were mounted with glass coverslips using Prolong Gold antifade mountant (Thermo Fisher Scientific, P36930). Imaging was performed using Leica SP8 confocal with ×63 objective (Leica) or SIM microscopy as described in detail below. Colocalization analysis and quantification was obtained with Velocity 3D Image Analysis Software (PerkinElmer).

Assessment of internalized SDC2–DEP1 complex and SDC2–VEGFR2 and DEP1–VEGFR2 complex in Rab5 early endosomes. HUVECs were plated on gelatin-coated 20-mm glass-bottom plates (Cellvis, D29–20–1.5-N). After transfection with the indicated adenovirus, cells were starved overnight in Opti-MEM and then placed on ice for 15 min to stop constitutive receptor internalization. For DEP1–SDC2 complex labeling, cells were incubated with 0.4 µM SNAP-Surface Alexa Fluor 488 substrate (New England Biolabs, S9129S) and a mouse anti-HA.11 (Covance, MMS-101P, 1:200) diluted in starvation media for 30 min on ice, and then cells were washed with cold PBS. For DEP1 or SDC2 and VEGFR2–Rab5 complex labeling, cells were incubated with a mouse anti-HA.11 (Covance, MMS-101P, 1:200) and an antibody against the extracellular domain of VEGFR2 (R&D, AF357, 1:100) diluted in starvation media for 20 min on ice, and then they were washed with cold PBS. Cells were then stimulated with prewarmed media containing 50 ng ml^{-1} VEGFA165 at 37 °C for 20 min to induce antibody-bound proteins internalization. After stimulation, residual antibody on the cell surface was removed by washing cells with cold acidic PBS (pH 2.5), and cells were then processed for immunocytochemistry.

For evaluation of constitutive endocytosis of DEP1 and DEP1–SDC2 complexes, HUVECs were first silenced for Sdc2 for 48 h. Cells were then seeded in gelatin-coated 20-mm glass-bottom plates and infected with DEP1-HA or DEP1-HA and SDC2-SNAP adenovirus for 48 h. After transfection, cells were kept overnight in Opti-MEM and then labeled with the indicated antibody at room temperature for 20 min. Cells were then placed in incubator at 37 °C. At the indicated time point (0 min, 15 min, 30 min and 1 h), cells were washed twice with cold acidic PBS (pH 2.5), and cells were then processed for immunocytochemistry.

Assessment of internalized DEP1 and VEGFR2 in mouse ECs. Mouse primary cells were isolated from lung or heart of WT or Sdc2$^{-/-}$ mice. Cells were plated on fibronectin-coated 35-mm glass-bottom dishes and infected for 48 h with 10 µl media from 293 A infected with adenovirus expressing human DEP1-HA-tagged protein. After overnight starvation, cells were incubated with anti-HA-tag rabbit

antibody (Cell Signaling Technology, 3724, 1:100) and with an antibody against the extracellular domain of mouse VEGFR2 (Flk1) (BD Pharmingen, 555307, 1:100) diluted in starvation media for 15 min on ice and then washed with cold PBS. Cells were then stimulated with prewarmed media containing 50 ng ml^{-1} VEGFA165 at 37 °C for 20 min, to induce antibody-bound DEP1 and VEGFR2 internalization and trafficking. Cells were then processed for differential labeling of cell surface and internalized proteins as described in Carrodus et al.,2014[54]. Briefly, cells were washed twice with PBS and fixed with 4% PFA for 10 min. After an additional wash with PBS, cells were blocked in 5%BSA (in PBS) for 30 min at room temperature. To label superficial DEP1-HA expression, un-permeabilized cells were incubated for 1 hour at room temperature in 1% BSA (in PBS) containing anti-rabbit IgG Alexa Fluor 568 (Thermo Fisher Scientific, A10042, 1:400) secondary antibody. After PBS wash, cells were incubated overnight at room temperature with an unlabeled secondary antibody raised against the species in which the primary antibody was raised. AffiniPure Fab fragment goat anti-rat IgG (H + L) (Jackson ImmunoResearch, 112.005.003, 0.13 mg ml^{-1}) was used to block superficial anti-VEGFR2 primary antibody, whereas AffiniPure Fab fragment goat anti-rabbit IgG (H + L) (Jackson ImmunoResearch, 111.005.144, 0.13 mg ml^{-1}) was used to block any superficial anti-HA primary antibody that was not fully bound by the labeled secondary antibody. The day after, cells were washed in PBS twice and postfixed in 4% PFA for 5 min at room temperature. Cells were then permeabilized and blocked with 5% BSA (in PBS) containing 0.1% Triton-X-100 at room temperature for 30 min. To label internalized proteins, cells were incubated for 1 hour at room temperature in 1% BSA (in PBS) containing the following secondary antibodies: an anti-Rat IgG Alexa Fluor-647 (Thermo Fisher Scientific, A-21472, 1:400) was used for internalized VEGFR2 labeling, and a second anti-rabbit fluorescently-conjugated secondary antibody tagged with a different fluorophore was used to label internalized DEP1-HA protein, in this case anti-rabbit IgG Alexa Fluor 488 (Thermo Fisher Scientific, A-21206, 1:400). Cell nuclei were counterstained with DAPI (Thermo Fisher Scientific, 62248, 1:1,000) for 5 min at room temperature. After washing in PBS, cells were mounted with glass coverslips using Prolong Gold antifade mountant (Thermo Fisher Scientific, P36930). Imaging was performed using Leica SP8 confocal with X63 objective (Leica).

SIM. SIM images were acquired on the OMX version 3 system (Applied Precision) using a U-PLANAPO ×60/1.42 PSF, oil immersion objective lens (Olympus) and CoolSNAP HQ2 charge-coupled device cameras with a pixel size of 0.080 mm (Photometrics). Samples were illuminated with 488-, 561- and 642-nm solid-state lasers (Coherent and MPB Communications) and acquired as described before[29]. Raw images were processed, reconstructed and aligned to reveal structures with resolutions of 100–125 nm using Softworx software (Applied Precision). Colocalization analysis and quantification was obtained with Velocity 3D Image Analysis Software (PerkinElmer).

Vesicles colocalization measurements. To measure protein colocalization inside Rab5$^+$ endosomes, we combined an object-based quantification method with a pixel-based method using Volocity software (PerkinElmer). We first segmented the images into objects and preprocessed the images to correct background noise and illumination. Only objects with standard deviation (SD) = 2.5 as lower threshold limit and minimum object size equal to 0.1 μm^2 were selected. Objects were then filtered by two interactions of dilation and excluded by size; objects with a size smaller than 0.25 μm^3 were excluded. Next, we measured the colocalization inside all the objects of the image by comparing the pixel intensities of the different channels and determining the correlation between them using the Pearson's correlation coefficient, either manually setting the threshold to 1,500 arbitrary units (AU) or following automated threshold calculation based on Costes et al., 2004. For line profile measurements, we drew a line across the selected object to show an overlay displaying the intensities of each channel along that line, illustrating the distance between DEP1, Sdc2 and Rab5 or DEP1, Sdc2 and VEGFR2 inside the selected endosome.

bEnd.3 cell in vitro permeability, proliferation and migration. Permeability and proliferation assays were performed with the xCELLigence RTCA System (Agilent), which allows measurement of electrical resistance of the culture plates surface over time. For the permeability assay, 30,000 bEnd.3 cells well were seeded onto the E-Plate 16 (Agilent, 5469830001) in DMEM containing 5% FBS. After ~ 60 h, rabbit IgG (5 μg ml^{-1}) or Sdc2 pAb (5 μg ml^{-1}) was added to plate wells, followed by $VEGFA_{165}$ stimulation (100 ng ml^{-1}). Permeability curves showed changes in electrical resistance (cell index) following $VEGFA_{165}$-induced EC monolayer permeability (cell index was measured every 15 min). For the proliferation assay, 5,000 bEnd.3 cells were seeded in E16 plates in DMEM containing 5% FBS in the presence of either rabbit IgG (5 μg ml^{-1}) or Sdc2 pAb (5 μg ml^{-1}) and VEGFA165 (100 ng ml^{-1}). Proliferation curves show ~50 h of monitoring (cell index is measured every 15 min).

EC migration was assessed using an in vitro wound-healing assay as previously reported[52]. Briefly, cells were seeded on Ibidi-culture inserts (Ibidi, 80209) to create a wound between two adjacent EC monolayers. At confluency, inserts were removed, and cells were allowed to migrate. Pictures of wound width were taken before and after stimulation (8 h), and wound closure (percentage) was calculated.

Antibody generation and direct enzyme-linked immunosorbent assay. A custom Sdc2 polyclonal antibody was generated by immunization of rabbits with a peptide corresponding to DEP1-binding motif of mouse Sdc2 (AA 124–141) and purified via affinity chromatography (GenScript).

For direct enzyme-linked immunosorbent assays, 96-well plates (Thermo Fisher Scientific, 15041) were coated overnight with increasing amounts of recombinant mouse Sdc2 (R&D Systems, 6585-SD-050) or mouse Sdc4 (R&D Systems, 6267-SD-050). Plates were incubated with Sdc2 pAb (5 μg ml^{-1}) for 1 h at room temperature followed by secondary anti-rabbit horseradish peroxidase for 1 h and chemiluminescence detection.

Assessment of vascular permeability in vivo. For assessment of stimuli-induced permeability we used Miles assay (skin permeability). Briefly, anesthetized mice were injected i.v. with 50 μl 2% Evans blue saline solution (sterile). After 10 min, vascular permeability was induced with intradermal injections of a 50-μl bolus of $VEGFA_{165}$ (200 ng) or histamine (Sigma-Aldrich, H7250, 100 μM) on one side of shaved back skin. The opposite side was injected with PBS (control). After 30 min ($VEGFA_{165}$) or 15 min (histamine), mice were euthanized, and skin around injection sites was excised and placed in tubes with 1 ml formamide for extraction of Evans blue (55 °C for 3 days). Extracted Evans blue was quantified with a spectrophotometer reader at 620 nm absorbance.

For baseline vascular permeability, mice were injected with 50 μl 2% Evans blue saline solution (sterile) and allowed to circulate for 30 min. Mice were euthanized and gravity-perfused with PBS (30 ml), and then samples from organs were collected and weighted. Samples were then placed in tubes with 1 ml formamide to extract leaked Evans blue as described for the Miles assay.

Cornea pocket assay. Slow-releasing pellets containing $VEGFA_{165}$ were surgically implanted into the mouse cornea[55,56], and IgG or Sdc2 pAb was injected systemically after 1 h from pellet implantation. One week after pellet implantation, eyeballs were collected, and corneas were dissected and immunostained with anti-mouse CD31 antibody (R&D Systems, AF3628, 1:200 dilution) to quantify neovessel formation with ImageJ (NIH).

Stroke model (permanent occlusion model). All mouse experimental protocols have been approved by the Institutional Animal Care & Use Committee at Yale University. The authors have complied with all relevant animal testing and research ethical regulations.

Mice were anesthetized with ketamine/xylazine and kept on warm water recirculating heating pad during all procedure. Mouse eyes were protected from corneal damages during a surgery using an ophthalmic lubricating ointment. Buprenorphine was given 20 min before surgery to induce preemptive analgesia. An incision was made between the left eye and ear under an operating microscope, and the temporal muscle was cut and divided exposing the left lateral aspect of the skull. Local incision was infiltrated with a local anesthetic (bupivacaine). The MCA and branches were identified through the semitranslucent skull, and a small burr hole was made using a high-speed microdrill, leaving the dura intact. Saline was applied to the area throughout the procedure to prevent heat injury, keeping the area always hydrated. A permanent focal stroke model was induced by MCA occlusion using 11-0 suture ligation. The incision was closed by two layers. After 24 h from stroke onset, mice were euthanized, brains were extracted ad quickly sectioned with a brain matrix (1 mm sections) and TTC live staining was performed. For mouse treatment, either rabbit IgG (100 μg per mouse) or Sdc2 pAb (100 μg per mouse) was injected i.v. 1 h before (prevention) or 1 h after stroke (therapy) surgery.

Stroke model (transient MCA occlusion model). The in vivo protocol was approved by the Institutional Animal Care & Use Committee of Yale University. All procedures were performed following these enforced guidelines and regulations and compliance with the Animal Research: Reporting of In vivo Experiments (ARRIVE) guidelines.

Preemptive buprenorphine was given 30 min before this surgical procedure. Anesthesia was induced with an intraperitoneal injection of ketamine (8.7 mg ml^{-1}) and xylazine (2 mg ml^{-1}). The body temperature was kept constant at 37.4 ± 1 °C using a water-circulating heating pad. All surgical manipulations were performed under aseptic conditions. Lidocaine (2%) was injected subcutaneously before the midline incision was made in the neck. Under a Zeiss dissecting microscope, submandibular glands were bluntly dissected to expose the right common carotid artery (CCA), the proximal external carotid artery (ECA) and the proximal segment of the internal carotid artery (ICA). The distal ECA was permanently ligated with 6-0 silk. The ICA and CCA were temporarily tightened with a 6-0 silk. After an arteriotomy was performed at the proximal ECA, the 6-0 silicone rubber-coated monofilament was introduced into the ECA and advanced to occlude the MCA via the right ICA for 45 min. The filament was withdrawn for the MCA reperfusion. The neck incision was closed with 6-0 prolene. Once on sternal, the animal was returned to the home cage on a heating pad until fully conscious. Sham-operated animals underwent the surgical procedure with permanent ligation of the ECA and branches but without intravascular intervention with the filament. 0.1 ml antibody or vehicle was given 30 min after reperfusion via direct injection into the right jugular vein. 0.3 ml of saline was injected intraperitoneally to prevent dehydration 2 h after ischemia/reperfusion injury.

MRI scanning. Mice were anesthetized during the MRI with ~1% isoflurane. Breathing rate was measured by placement of a respiration pad under the torso, and temperature was monitored through a rectal fiber-optic probe thermometer.

MRI data were acquired on a 11.74 T horizontal-bore Bruker Avance system interfaced with Bruker ParaVision v6.0.1 software (Billerica) using ^{1}H volume coil (4 cm). Shimming was done using an ellipsoid region to bring the water linewidth to less than 30 Hz using B0 mapping with second-order shim. T2-weighted anatomical MRI was first performed using a spin-echo sequence in axial orientation (Field of View (FOV)): 19.2 × 19.2 mm3, 128 × 128 in-plane resolution) with TR (repetition time)/TE (echo time) = 2,500/25 ms with slice thickness of 1 mm. T2 mapping was based on multi-echo sequence with 10 echo times (10–100 ms) with TR = 4,000 ms) with the same FOV and in-plane resolution as T2-weighted anatomical MRI. The multiple echo times enabled voxel-wise calculations of T2 values. Voxel-wise T2 maps were calculated by fitting MRI voxel intensities versus the series of TE values to a monoexponential curve e − TE/T2. Diffusion weighted (spin-echo planar (SE-EPI)) imaging was performed with TR/TE = 4,000/26.18 ms, FOV: 19.2 × 19.2 mm^3, 128 × 128 in-plane resolution and slice thickness 1 mm to assess ischemically injured tissue and edema. We used three directions and six b values (0, 50, 100, 250, 500 and 1,000 s/mm^2) with voxel-wise calculated quantitative apparent diffusion coefficient (ADC) maps.

Noninvasive quantitative cerebral blood flow was carried out to identify the perfusion deficit on 1-mm-thick slices throughout the MCA occlusion region using a form of pseudo-continuous arterial spin labeling, flow-alternating inversion recovery MRI. The sequence employs a spin-echo EPI imaging module (TR/TE = 10,000/14 ms, FOV = 32 × 32 mm^3, 85 × 85 matrix size, 1 mm slice thickness with 1 mm gap). Voxel-based analysis generated using codes written in MATLAB (MathWorks) allowed unbiased analysis of the spatial, volumetric and dynamic evaluation of different tissue compartments. Tissue was compartmentalized using in-house defined thresholds set for two parameters: (1) T2 and R2 (1/T2) signal change and ADC and (2) ADC and cerebral blood flow dataset for diffusion/perfusion mismatch. Color-coded images were created enabling analysis of changes in voxel distribution across ischemic core, penumbra/edema and nonischemic tissue. Lesion and hemispheric volumes were determined on T2-weighted images. The hemispheres were traced manually on each slice. The position of the midline was determined with the use of the following neuroanatomic landmarks: falx cerebri, corpus pineale, fissura longitudinalis, infundibulum, aqueductus cerebri and third ventricle as described by Gerriets et al.[57]. Lesion volumes were determined from ADC maps by tracing of the hypointense lesions. The areas were then summed and multiplied by the slice thickness. Lesion volumes were calculated with and without edema correction and expressed as percentage of the hemispheric volume[57].

Reporting Summary. Further information on research design is available in the Nature Research Reporting Summary linked to this article.

Data availability

All data supporting the findings of this study are available within the paper and associated files. Source data are provided with this paper.

Received: 13 August 2021; Accepted: 6 April 2022;
Published online: 16 May 2022

References

1. Bates, D. O. Vascular endothelial growth factors and vascular permeability. *Cardiovasc Res.* **87**, 262–271 (2010).
2. Park-Windhol, C. & D'Amore, P. A. Disorders of vascular permeability. *Annu. Rev. Pathol.* **11**, 251–281 (2016).
3. Claesson-Welsh, L., Dejana, E. & McDonald, D. M. Permeability of the endothelial barrier: identifying and reconciling controversies. *Trends Mol. Med.* **27**, 314–331 (2021).
4. van Bruggen, N. et al. VEGF antagonism reduces edema formation and tissue damage after ischemia/reperfusion injury in the mouse brain. *J. Clin. Invest.* **104**, 1613–1620 (1999).
5. Croll, S. D. et al. VEGF-mediated inflammation precedes angiogenesis in adult brain. *Exp. Neurol.* **187**, 388–402 (2004).
6. Barratt, S., Medford, A. R. & Millar, A. B. Vascular endothelial growth factor in acute lung injury and acute respiratory distress syndrome. *Respiration* **87**, 329–342 (2014).
7. Sharp, C., Millar, A. B. & Medford, A. R. Advances in understanding of the pathogenesis of acute respiratory distress syndrome. *Respiration* **89**, 420–434 (2015).
8. Orsenigo, F. et al. Phosphorylation of VE-cadherin is modulated by haemodynamic forces and contributes to the regulation of vascular permeability in vivo. *Nat. Commun.* **3**, 1208 (2012).
9. Sun, Z. et al. VEGFR2 induces c-Src signaling and vascular permeability in vivo via the adaptor protein TSAd. *J. Exp. Med.* **209**, 1363–1377 (2012).
10. Simons, M., Gordon, E. & Claesson-Welsh, L. Mechanisms and regulation of endothelial VEGF receptor signalling. *Nat. Rev.* **17**, 611–625 (2016).
11. Smith, R. O. et al. Vascular permeability in retinopathy is regulated by VEGFR2 Y949 signaling to VE-cadherin.*Elife* **9**, e54056 (2020).
12. Eliceiri, B. P. et al. Selective requirement for Src kinases during VEGF-induced angiogenesis and vascular permeability. *Mol. Cell* **4**, 915–924 (1999).
13. Paul, R. et al. Src deficiency or blockade of Src activity in mice provides cerebral protection following stroke. *Nat. Med.* **7**, 222–227 (2001).
14. Gavard, J. & Gutkind, J. S. VEGF controls endothelial-cell permeability by promoting the beta-arrestin-dependent endocytosis of VE-cadherin. *Nat. Cell Biol.* **8**, 1223–1234 (2006).
15. Elias, B. C. et al. Phosphorylation of Tyr-398 and Tyr-402 in occludin prevents its interaction with ZO-1 and destabilizes its assembly at the tight junctions. *J. Biol. Chem.* **284**, 1559–1569 (2009).
16. Fantin, A. et al. VEGF165-induced vascular permeability requires NRP1 for ABL-mediated SRC family kinase activation. *J. Exp. Med.* **214**, 1049–1064 (2017).
17. Gitay-Goren, H., Soker, S., Vlodavsky, I. & Neufeld, G. The binding of vascular endothelial growth factor to its receptors is dependent on cell surface-associated heparin-like molecules. *J. Biol. Chem.* **267**, 6093–6098 (1992).
18. Chiodelli, P., Bugatti, A., Urbinati, C. & Rusnati, M. Heparin/Heparan sulfate proteoglycans glycomic interactome in angiogenesis: biological implications and therapeutical use. *Molecules* **20**, 6342–6388 (2015).
19. Corti, F. et al. N-terminal syndecan-2 domain selectively enhances 6-O heparan sulfate chains sulfation and promotes VEGFA165-dependent neovascularization. *Nat. Commun.* **10**, 1562 (2019).
20. Ferrara, N. Binding to the extracellular matrix and proteolytic processing: two key mechanisms regulating vascular endothelial growth factor action. *Mol. Biol. Cell* **21**, 687–690 (2010).
21. Li, X. et al. VEGFR2 pY949 signalling regulates adherens junction integrity and metastatic spread. *Nat. Commun.* **7**, 11017 (2016).
22. Brash, J. T. Evaluating vascular hyperpermeability-inducing agents in the skin with the Miles assay. *J. Vis. Exp.*(136), 57524.
23. Wang, Y. et al. Ephrin-B2 controls VEGF-induced angiogenesis and lymphangiogenesis. *Nature* **465**, 483–486 (2010).
24. Hayashi, M. et al. VE-PTP regulates VEGFR2 activity in stalk cells to establish endothelial cell polarity and lumen formation. *Nat. Commun.* **4**, 1672 (2013).
25. Grazia Lampugnani, M. et al. Contact inhibition of VEGF-induced proliferation requires vascular endothelial cadherin, beta-catenin, and the phosphatase DEP-1/CD148. *J. Cell Biol.* **161**, 793–804 (2003).
26. Fournier, P. et al. The protein tyrosine phosphatase PTPRJ/DEP-1 contributes to the regulation of the Notch-signaling pathway and sprouting angiogenesis. *Angiogenesis* **23**, 145–157 (2020).
27. Lanahan, A. A. et al. PTP1b is a physiologic regulator of vascular endothelial growth factor signaling in endothelial cells. *Circulation* **130**, 902–909 (2014).
28. Corti, F. & Simons, M. Modulation of VEGF receptor 2 signaling by protein phosphatases. *Pharmacol. Res.* **115**, 107–123 (2017).
29. Lanahan, A. A. et al. VEGF receptor 2 endocytic trafficking regulates arterial morphogenesis. *Dev. Cell* **18**, 713–724 (2010).
30. Ostman, A., Yang, Q. & Tonks, N. K. Expression of DEP-1, a receptor-like protein-tyrosine-phosphatase, is enhanced with increasing cell density. *Proc. Natl. Acad. Sci. U S A* **91**, 9680–9684 (1994).
31. Takahashi, T. et al. Endothelial localization of receptor tyrosine phosphatase, ECRTP/DEP-1, in developing and mature renal vasculature. *J. Am. Soc. Nephrol.* **10**, 2135–2145 (1999).
32. Adam, A. P. Regulation of endothelial adherens junctions by tyrosine phosphorylation.*Mediators Inflamm.* **2015**, 272858 (2015).
33. Whiteford, J. R. et al. Syndecan-2 is a novel ligand for the protein tyrosine phosphatase receptor CD148. *Mol. Biol. Cell* **22**, 3609–3624 (2011).
34. Kofler, N. et al. The Rab-effector protein RABEP2 regulates endosomal trafficking to mediate vascular endothelial growth factor receptor-2 (VEGFR2)-dependent signaling. *J. Biol. Chem.* **293**, 4805–4817 (2018).
35. Srinivasan, B. & Kolli, A. R. in *Blood-Brain Barrier* (ed. Barichell, T.) 99–114 (Springer, 2019).
36. Lange, C., Storkebaum, E., de Almodovar, C. R., Dewerchin, M. & Carmeliet, P. Vascular endothelial growth factor: a neurovascular target in neurological diseases. *Nat. Rev. Neurol.* **12**, 439–454 (2016).
37. Apte, R. S., Chen, D. S. & Ferrara, N. VEGF in signaling and disease: beyond discovery and development. *Cell* **176**, 1248–1264 (2019).
38. Simard, J. M., Kent, T. A., Chen, M., Tarasov, K. V. & Gerzanich, V. Brain oedema in focal ischaemia: molecular pathophysiology and theoretical implications. *Lancet Neurol.* **6**, 258–268 (2007).
39. Ma, Y., Zechariah, A., Qu, Y. & Hermann, D. M. Effects of vascular endothelial growth factor in ischemic stroke. *J. Neurosci. Res.* **90**, 1873–1882 (2012).
40. Geiseler, S. J. & Morland, C. The Janus face of VEGF in stroke.*Int. J. Mol. Sci.* **19**, 1362 (2018).
41. Doyle, K. P. & Buckwalter, M. S. A mouse model of permanent focal ischemia: distal middle cerebral artery occlusion. *Methods Mol. Biol.* **1135**, 103–110 (2014).

42. Jin, Z. G. et al. Ligand-independent activation of vascular endothelial growth factor receptor 2 by fluid shear stress regulates activation of endothelial nitric oxide synthase. *Circ. Res.* **93**, 354–363 (2003).
43. Warren, C. M. A ligand-independent VEGFR2 signaling pathway limits angiogenic responses in diabetes. *Sci. Signal.* **7**, ra1 (2014).
44. Couchman, J. R., Gopal, S., Lim, H. C., Norgaard, S. & Multhaupt, H. A. Fell-Muir Lecture: Syndecans: from peripheral coreceptors to mainstream regulators of cell behaviour. *Int. J. Exp. Pathol.* **96**, 1–10 (2015).
45. De Rossi, G. et al. Pathological angiogenesis requires Syndecan-4 for efficient VEGFA-induced VE-Cadherin internalization. *Arter. Thromb. Vasc. Biol.* **41**, 1374–1389 (2021).
46. Dews, I. C. & Mackenzie, K. R. Transmembrane domains of the syndecan family of growth factor coreceptors display a hierarchy of homotypic and heterotypic interactions. *Proc. Natl. Acad. Sci. U S A* **104**, 20782–20787 (2007).
47. Ruiz, X. D. et al. Syndecan-2 is a novel target of insulin-like growth factor binding protein-3 and is over-expressed in fibrosis. *PLoS One* **7**, e43049 (2012).
48. Choi, S. et al. Inflammatory hypoxia induces syndecan-2 expression through IL-1beta-mediated FOXO3a activation in colonic epithelia. *FASEB J.* **31**, 1516–1530 (2017).
49. Hong, H. et al. Up-regulation of syndecan-2 in proximal colon correlates with acute inflammation. *FASEB J.* **33**, 11381–11395 (2019).
50. Zhang, Z. G. et al. VEGF enhances angiogenesis and promotes blood-brain barrier leakage in the ischemic brain. *J. Clin. Invest.* **106**, 829–838 (2000).
51. Reeson, P. et al. Delayed inhibition of VEGF signaling after stroke attenuates blood-brain barrier breakdown and improves functional recovery in a comorbidity-dependent manner. *J. Neurosci.* **35**, 5128–5143 (2015).
52. Corti, F., Finetti, F., Ziche, M. & Simons, M. The Syndecan-4/protein kinase C alpha pathway mediates prostaglandin E-2-induced extracellular regulated kinase (ERK) activation in endothelial cells and angiogenesis in vivo. *J. Biol. Chem.* **288**, 12712–12721 (2013).
53. Schneider, C. A., Rasband, W. S. & Eliceiri, K. W. NIH Image to ImageJ: 25 years of image analysis. *Nat. Methods* **9**, 671–675 (2012).
54. Carrodus, N. L. et al. Differential labeling of cell-surface and internalized proteins after antibody feeding of live cultured neurons. *J. Vis. Exp.* e51139 (2014).
55. Tang, Z. et al. A mouse model of the cornea pocket assay for angiogenesis study. *J. Vis. Exp.* **54**, 3077 (2011).
56. Ziche, M. & Morbidelli, L. The corneal pocket assay. *Methods Mol. Biol.* **1214**, 15–28 (2015).
57. Gerriets, T. et al. Noninvasive quantification of brain edema and the space-occupying effect in rat stroke models using magnetic resonance imaging. *Stroke* **35**, 566–571 (2004).
58. Kovalenko, M. et al. Site-selective dephosphorylation of the platelet-derived growth factor beta-receptor by the receptor-like protein-tyrosine phosphatase DEP-1. *J. Biol. Chem.* **275**, 16219–16226 (2000).
59. Persson, C., Engstrom, U., Mowbray, S. L. & Ostman, A. Primary sequence determinants responsible for site-selective dephosphorylation of the PDGF beta-receptor by the receptor-like protein tyrosine phosphatase DEP-1. *FEBS Lett.* **517**, 27–31 (2002).
60. Tarcic, G. et al. An unbiased screen identifies DEP-1 tumor suppressor as a phosphatase controlling EGFR endocytosis. *Curr. Biol.* **19**, 1788–1798 (2009).

Acknowledgements

We thank D. Chen for the technical assistance and helpful discussion regarding the corneal pocket assay and confocal imaging. This work was supported by grants from National Institute of Health (NIH) HL149343 and HL062289 to Michael Simons.

Author contributions

F.C. designed and performed experiments, analyzed data and wrote manuscript. E.R. designed/performed experiments and analyzed data. R.-M.F. performed experiments and analyzed data. T.D. designed experiments and analyzed data. J.Z., Z.W.Z. and J.M., performed experiments. M.S. designed experiments, analyzed data and wrote the manuscript.

Competing interests

The authors declare no competing interests.

Additional information

Extended data is available for this paper at https://doi.org/10.1038/s44161-022-00064-2.

Supplementary information The online version contains supplementary material available at https://doi.org/10.1038/s44161-022-00064-2.

Correspondence and requests for materials should be addressed to M. Simons.

Peer review information *Nature Cardiovascular Research* thanks Christiana Ruhrberg, Philipp Berger and the other, anonymous, reviewer(s) for their contribution to the peer review of this work.

Reprints and permissions information is available at www.nature.com/reprints.

Publisher's note Springer Nature remains neutral with regard to jurisdictional claims in published maps and institutional affiliations.

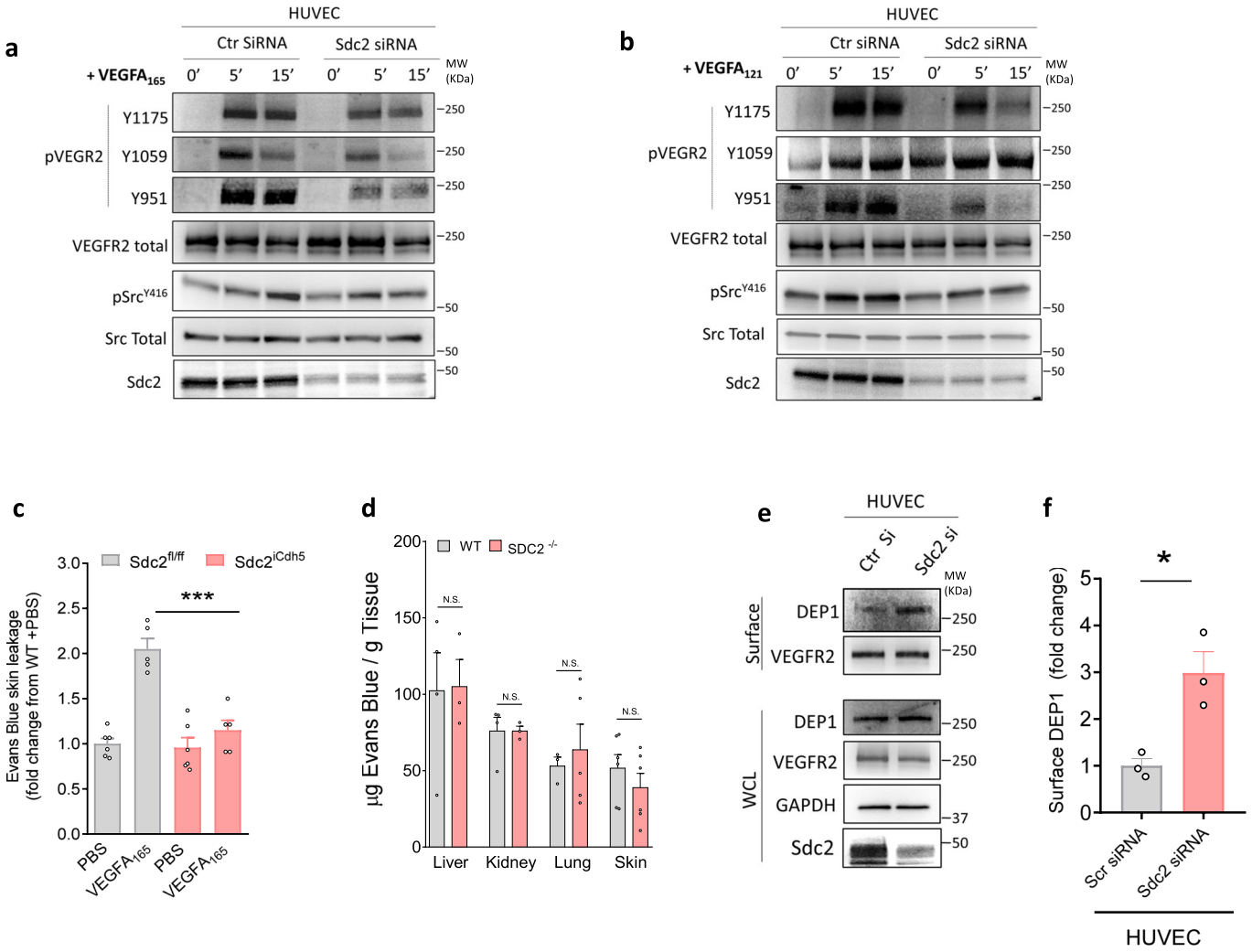

Extended Data Fig. 1 | a-b, western blot analysis of VEGFR2 phosphorylation (pVEGFR2) following stimulation with $VEGFA_{165}$ (50 ng/ml) or $VEGFA_{121}$ (50 ng/ml) in Control (Ctr Si) vs. Sdc2-depleted (Sdc2 siRNA) HUVEC. **c**, $VEGFA_{165}$ -induced Evans blue leakage in the back skin of WT vs $Sdc2^{iECKO}$ mice (n = 5–6) (representative blots of 3 independent experiments). **d**, evaluation of baseline permeability in various organs measured as Evans blue dye leakage in Wild type (WT) vs $Sdc2^{-/-}$ mice (n = 3–6). **e, f** western blot analysis of cell surface protein levels in Control (Ctr) vs. Sdc2-depleted (Sdc2 siRNA) HUVEC (n = 3). Data are presented as mean values +/- SEM (standard error of the mean). In all figure panels, each dot represents a biological independent experiment (n). Statistical analysis was performed by one-way ANOVA with Sidak's multiple comparison test (panels c, d), and by unpaired t-student test (panel f), (N.S. not significant, * $P < 0.05$, ** $P < 0.01$, *** $P < 0.001$).

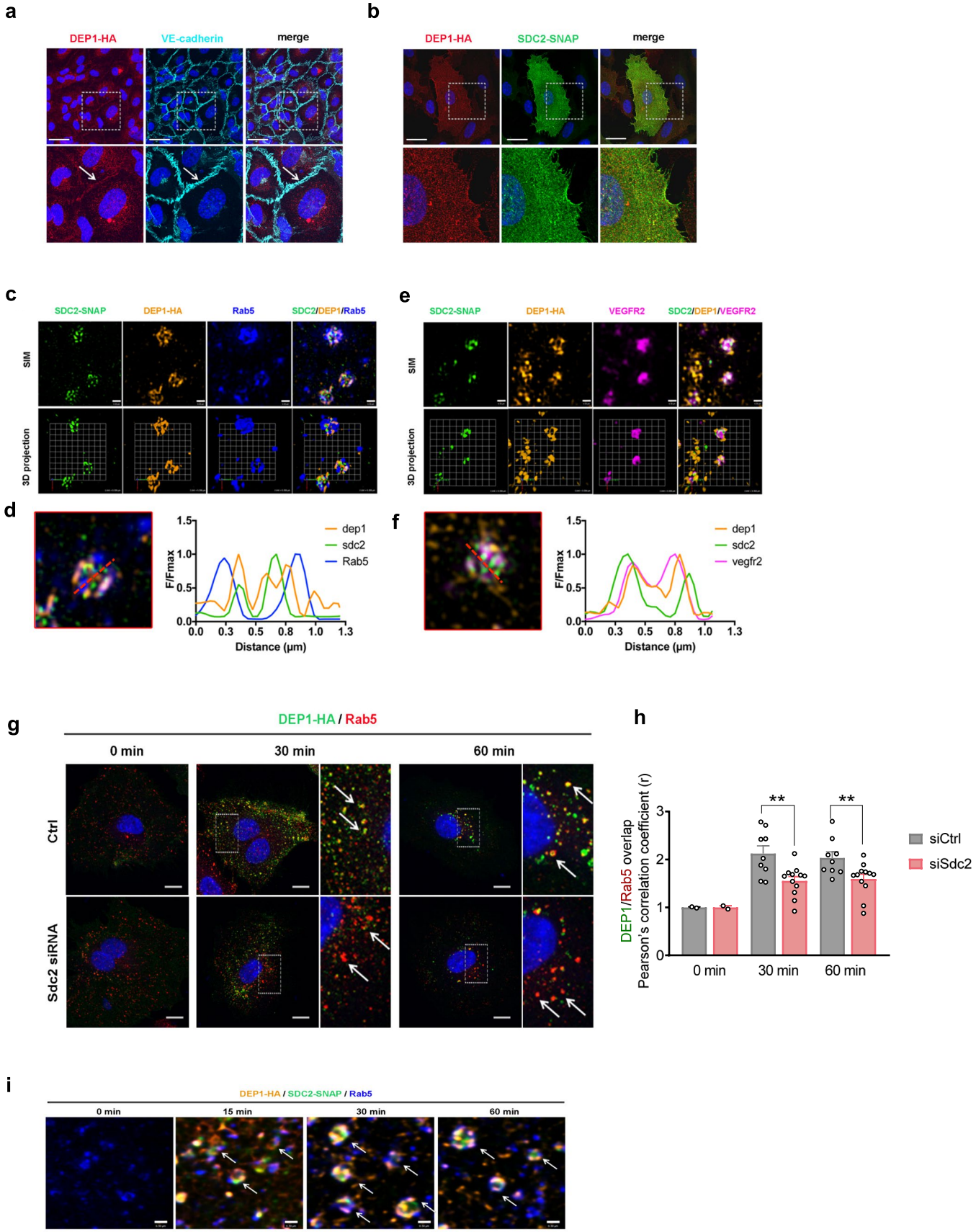

Extended Data Fig. 2 | See next page for caption.

Extended Data Fig. 2 | a, confocal image of confluent HUVEC cells in basal conditions showing human DEP1 carrying N-terminal HA-tag (DEP1-HA, red) expression at cell–cell junctions labeled with VE-cadherin (cyan), white arrows, lower panels. Scale bar: 25 μm. **b**, confocal image of HUVEC cells in basal conditions expressing both human DEP1 carrying N-terminal HA-tag (DEP1-HA, red) and human Sdc2 carrying N-terminal SNAP-tag (SDC2-SNAP, green) proteins. Lower panels show magnification of box in upper panels showing localization of both proteins at the plasma membrane and at the membrane protrusions. Scale bar: 25 μm. **c, f**, SIM imaging of SDC2/DEP1/Rab5 and SDC2/DEP1/VEGFR2 complexes in HUVECs expressing DEP1-HA and SDC2-SNAP proteins and treated for 20 min with 50 ng/ml $VEGFA_{165}$. Scale bar: 0.5 μm. **d,f**, line profile analysis illustrating the distance between DEP1, Sdc2 and Rab5 or DEP1, Sdc2 and VEGFR2 in the same compartment. Plots represent the fluorescent signal in SIM images as a function of position along the line profile in left panel (red dotted line). **g, h** confocal images of constitutive internalization of DEP1 after incubation for 0 min, 30 min and 60 min in absence of VEGFA in HUVECs control and HUVECs transfected with Sdc2 siRNA. Scale bar: 15 μm. **i**, confocal image of internalized SDC2–DEP1 complexes in Rab5+ endosomes (white arrows) following constitutive endocytosis in VEGFA-free media. Scale bar: 5 μm. All images are representative images of >3 independent experiments (n). Data are presented as mean values +/- SEM (standard error of the mean). Statistical analysis was performed by two-way ANOVA with Sidak's multiple comparison test (panels h), (N.S. not significant, * $P < 0.05$, ** $P < 0.01$, *** $P < 0.001$).

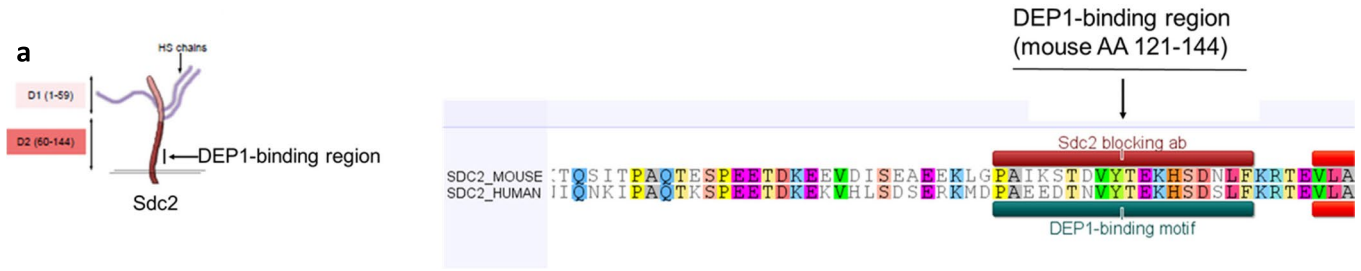

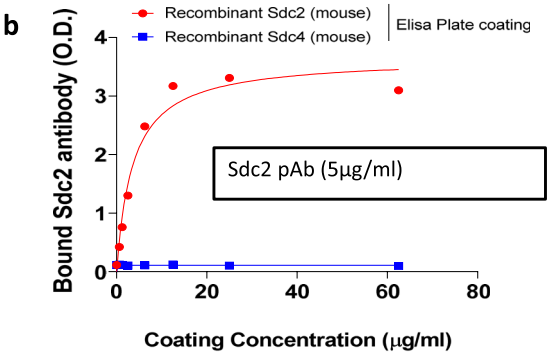

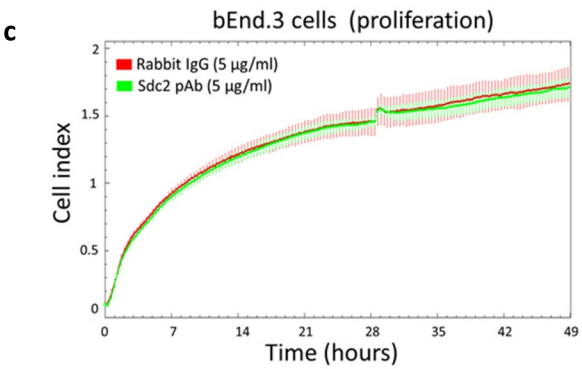

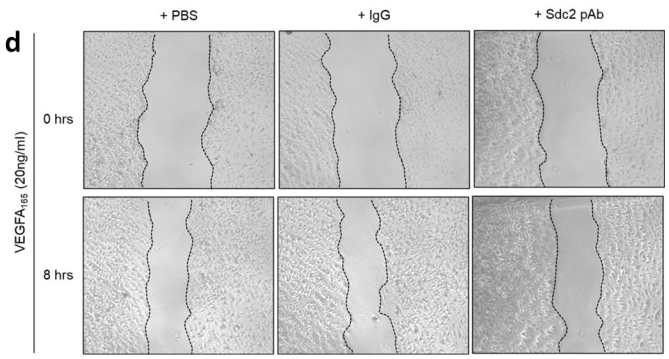

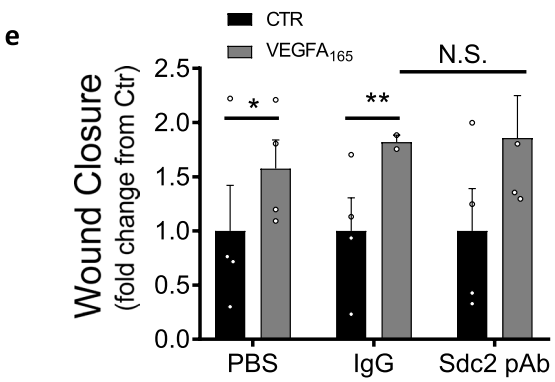

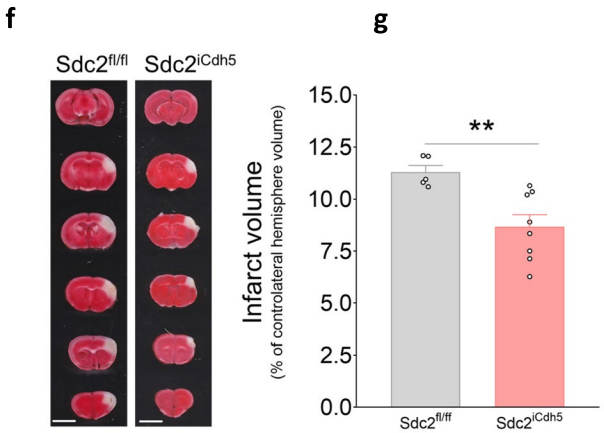

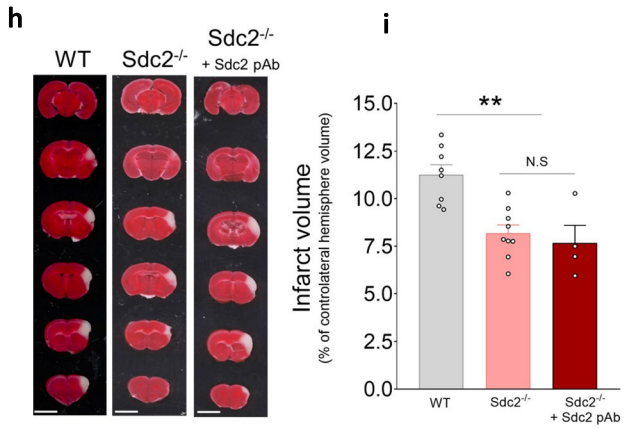

Extended Data Fig. 3 | a, position and sequence of DEP1-binding motif in human Sdc2. **b**, direct ELISA comparing Sdc2 pAb (5 µg/ml) binding to mouse Sdc2 vs. mouse Sdc4. **c**, bEnd.3 cell proliferation in presence of rabbit IgG (5 µg/ml) or Sdc2 pAb (5 µg/ml) measured with xCELLigence system. **d-e**, ECs migration measured by *in vitro* wound-healing assay in bEnd.3 cells in presence of rabbit IgG (5 µg/ml) or Sdc2 pAb (5 µg/ml) (n = 3–4) **f-g**, TTC staining (at 24 h post stroke) and quantification of stroke infarct in WT vs $Sdc2^{iECKO}$ (n = 5–8). **h-i**, TTC staining (at 24 h post stroke) in $Sdc2^{-/-}$ mice with or without Sdc2 pAb treatment (administered 1 hour before stroke) (n = 4–9). Data are presented as mean values +/- SEM (standard error of the mean). In all figure panels, each dot represents a biological independent experiment (n). Statistical analysis was performed by one-way ANOVA with Sidak's multiple comparison test (panels e, i), and by unpaired t-student test (panel g), (N.S. not significant, * $P < 0.05$, ** $P < 0.01$, *** $P < 0.001$).

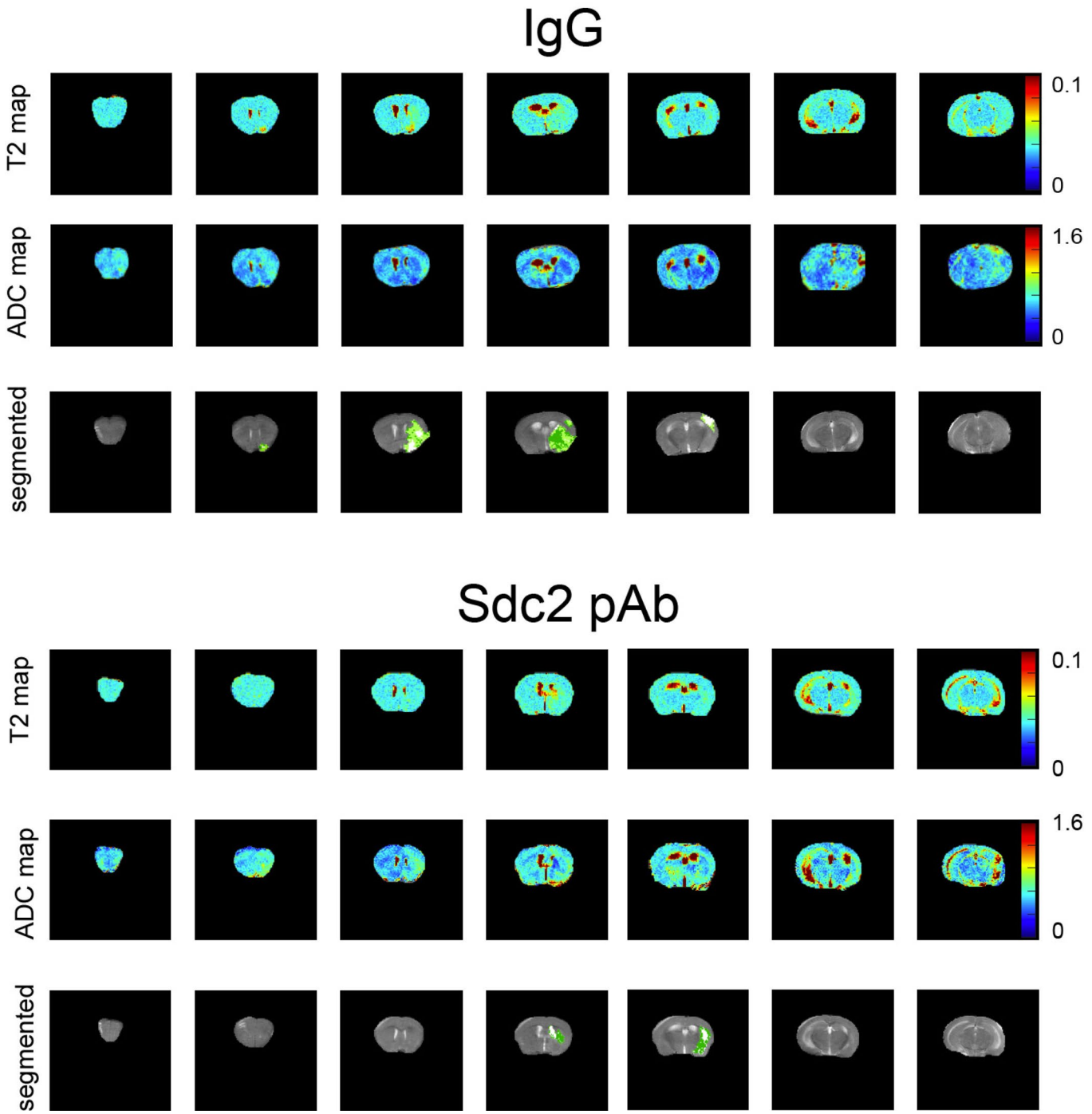

Extended Data Fig. 4 | MR imaging of IgG and Sdc2 pAb-treated mice: Representative T2 maps from mouse treated with IgG and Sdc2 pAb showing relatively well defined heterogeneous, hyperintense area within right MCA territory with measured T2 values in a range of 0.05–0.09 ms which were higher compared with contralateral normal tissue average 0.03 ms. On the ADC map, in the same region there is hypointense area with low ADC values, range from 0.4–0.8×10–3mm2/s, due to restricted diffusion. In normal appearing contralateral tissue measured ADC values were 0.9–1.1×10-3mm2/s. Compartmentalization analysis (see Material and Methods for details) shows different compartments of ischemic stroke; core (white), penumbra (light green) and edema (dark green).

nature portfolio

Corresponding author(s): Michael Simons

Last updated by author(s): Apr 4, 2022

Reporting Summary

Nature Portfolio wishes to improve the reproducibility of the work that we publish. This form provides structure for consistency and transparency in reporting. For further information on Nature Portfolio policies, see our Editorial Policies and the Editorial Policy Checklist.

Statistics

For all statistical analyses, confirm that the following items are present in the figure legend, table legend, main text, or Methods section.

n/a	Confirmed	
☐	☒	The exact sample size (*n*) for each experimental group/condition, given as a discrete number and unit of measurement
☐	☒	A statement on whether measurements were taken from distinct samples or whether the same sample was measured repeatedly
☐	☒	The statistical test(s) used AND whether they are one- or two-sided *Only common tests should be described solely by name; describe more complex techniques in the Methods section.*
☐	☒	A description of all covariates tested
☐	☒	A description of any assumptions or corrections, such as tests of normality and adjustment for multiple comparisons
☐	☒	A full description of the statistical parameters including central tendency (e.g. means) or other basic estimates (e.g. regression coefficient) AND variation (e.g. standard deviation) or associated estimates of uncertainty (e.g. confidence intervals)
☐	☒	For null hypothesis testing, the test statistic (e.g. *F*, *t*, *r*) with confidence intervals, effect sizes, degrees of freedom and *P* value noted *Give P values as exact values whenever suitable.*
☒	☐	For Bayesian analysis, information on the choice of priors and Markov chain Monte Carlo settings
☒	☐	For hierarchical and complex designs, identification of the appropriate level for tests and full reporting of outcomes
☒	☐	Estimates of effect sizes (e.g. Cohen's *d*, Pearson's *r*), indicating how they were calculated

Our web collection on statistics for biologists contains articles on many of the points above.

Software and code

Policy information about availability of computer code

Data collection	No software was used for data collection
Data analysis	N/A

For manuscripts utilizing custom algorithms or software that are central to the research but not yet described in published literature, software must be made available to editors and reviewers. We strongly encourage code deposition in a community repository (e.g. GitHub). See the Nature Portfolio guidelines for submitting code & software for further information.

Data

Policy information about availability of data

All manuscripts must include a data availability statement. This statement should provide the following information, where applicable:

- Accession codes, unique identifiers, or web links for publicly available datasets
- A description of any restrictions on data availability
- For clinical datasets or third party data, please ensure that the statement adheres to our policy

All data supporting the findings of this study are available within the paper and associated files. Source data are provided with this paper.This statement has been provided in the manuscript under a separate section called "Data availability"

Field-specific reporting

Please select the one below that is the best fit for your research. If you are not sure, read the appropriate sections before making your selection.

☒ Life sciences ☐ Behavioural & social sciences ☐ Ecological, evolutionary & environmental sciences

For a reference copy of the document with all sections, see nature.com/documents/nr-reporting-summary-flat.pdf

Life sciences study design

All studies must disclose on these points even when the disclosure is negative.

Sample size	Sample size calculation was not performed. Sample size was chosen in agreement with number commonly accepted within this field.
Data exclusions	No data exclusion
Replication	All details of replications are reported in figure legends
Randomization	Not applicable
Blinding	In vivo experiments were performed in blinded-manner. Blinding was not possible in vitro, experiments were performed by individual investigators.

Reporting for specific materials, systems and methods

We require information from authors about some types of materials, experimental systems and methods used in many studies. Here, indicate whether each material, system or method listed is relevant to your study. If you are not sure if a list item applies to your research, read the appropriate section before selecting a response.

Materials & experimental systems

n/a	Involved in the study
☐	☒ Antibodies
☐	☒ Eukaryotic cell lines
☒	☐ Palaeontology and archaeology
☐	☒ Animals and other organisms
☒	☐ Human research participants
☒	☐ Clinical data
☒	☐ Dual use research of concern

Methods

n/a	Involved in the study
☒	☐ ChIP-seq
☒	☐ Flow cytometry
☐	☒ MRI-based neuroimaging

Antibodies

Antibodies used	List of antibodies with application and dilutions (IHC, immunohistochemistry; WB; western blot): pVEGFR2 Y1175 (WB 1:1000, Cell Signaling #2478), pVEGFR2 Y1059 (for HUVEC, WB 1:1000, Cell Signaling #3817,), pVEGFR2 Y1059 (for mouse ECs, WB 1:1000, EMD Millipore #ABS553), pVEGFR2 Y951 (WB 1:1000, Cell Signaling #4991), VEGFR2 total (WB 1:1000, Cell Signaling #2479), VE-Cad (for HUVEC, WB 1:200, Santa Cruz #sc-9989 (F-8)), VE-Cad (for mouse ECs, WB 1:500, BD Pharmingen #555289), mouse Sdc2 (WB 1:200, R&D #AF6585 - polyclonal raised against mouse Sdc2 ED), human Sdc2 (WB 1:200, R&D # AF2965 , polyclonal raised against mouse human ED), mouse PTP1b (WB 1:200, Santa Cruz #sc-1718-R (N19-R)), human PTP1b (WB 1:500, BD Pharmingen #610139), VEPTP (VE-PTP-C pAb69 and VE-PTP 1-8 pAb70 were gifts from Prof. Dietmar Vestweber, Max Plank Institute for Molecular Biomedicine, Münster, Germany), DEP1 (WB 1:200, Santa Cruz #sc-21761 (143-41)) NRP1 (WB 1:1000, Cell signaling #3725,), HA-tag (WB 1:1000, Cell signaling #3724), rabbit anti-Rab5 (Cell Signaling, #3547, IHC 1:200); goat anti-VEGFR2 (R&D, #AF357, IHC 1:100); mouse anti-HA.11 (Covance, #MMS-101P, IHC 1:200); rabbit anti-HA (Cell signaling, #3724, IHC 1:200); rabbit anti-VE-cadherin (Cell Signaling, #2500, IHC 1:200); goat anti-mouse VE-cadherin (R&D Systems, #AF1002, IHC 1:100); rat anti-mouse Flk1 (BD, #555307, IHC 1:100).
Validation	Specificity of Sdc2 pAb was validated by direct ELISA assay (Extended data figure 3b) and functionally in vivo (Extended data figure 3h-i) . Commercial antibodies were validated by vendors for the application used in the manuscripts.

Eukaryotic cell lines

Policy information about cell lines

Cell line source(s)	Human Umbilical Vein Endothelial Cells (HUVEC) were obtained from Yale VBT tissue-culture core laboratory. Mouse primary endothelial cells were isolated from freshly collected mouse heart or lung tissues bEnd.3 cell line was purchased from ATCC (CRL-2299TM) 293A cell were purchased from Invitrogen (R70507)

Authentication	Commercial cell lines were not authenticated
Mycoplasma contamination	Cells were not tested for mycoplasma
Commonly misidentified lines (See ICLAC register)	None

Animals and other organisms

Policy information about studies involving animals; ARRIVE guidelines recommended for reporting animal research

Laboratory animals	All mouse experimental protocols have been approved by the Institutional Animal Care & Use Committee (IACUC) at Yale University. The authors have complied with all relevant animal testing and research ethical regulations. All transgenic mice used in this study has been previously described20: Sdc2 Knockout-first transgenic mice (Sdc2tm1a(KOMP)Wtsi), Sdc2 null mice (Sdc2-/-), Sdc2 conditional transgenic mice (Sdc2fl/fl), Sdc2 endothelial-specific knockout (sdc2icdh5). All animals were back-crossed at least 10 generation to a C57Black6/J strain. For this study male mice (Species: mus musculus) were used between age 9-15 weeks old. Mice were housed under 12hours light/12 hours dark cycle.
Wild animals	No wild animals were used in this study
Field-collected samples	No field collected samples were used in this study
Ethics oversight	All mouse experimental protocols have been approved by the Institutional Animal Care & Use Committee (IACUC) at Yale University. The authors have complied with all relevant animal testing and research ethical regulations. Rabbits were not used in this study. A policlonal antibody against Sdc2 (sdc2 pAb) was previously generated in rabbits by a external commercial company (Genscript).

Note that full information on the approval of the study protocol must also be provided in the manuscript.

Magnetic resonance imaging

Experimental design

Design type	Multimodal Magnetic Resonance Imaging
Design specifications	anatomical MRI, diffusion weighted MRI (DWI), perfusion weighted MRI using arterial spin labeling-flow sensitive alternating inversion recovery (FAIR)technique
Behavioral performance measures	*State number and/or type of variables recorded (e.g. correct button press, response time) and what statistics were used to establish that the subjects were performing the task as expected (e.g. mean, range, and/or standard deviation across subjects).*

Acquisition

Imaging type(s)	structural, diffusion, perfusion
Field strength	11.74T
Sequence & imaging parameters	T2 weighted anatomical MRI (Rapid Acquisition with Refocusing Echoes-RARE) sequence in axial orientation (FOV: 19.2×19.2 mm3, 128×128 in-plane resolution) with TR/TE=2500/25ms, slice thickness of 1 mm. T2 mapping was based on multi echo RARE sequence with 10 echo times TE (10−100 ms) with TR=4000 ms) with the same FOV and in plane resolution as T2 weighted anatomical MRI. Diffusion weighted (spin echo planar (SE-EPI)) imaging with TR/TE=4000/26.18 ms, FOV: 19.2×19.2 mm3, 128×128 in-plane resolution, slice thickness 1mm, 3 directions and 6 b values (0, 50, 100, 250, 500, 1000 s/mm2). ASL FAIR sequence employs a spin echo EPI imaging module (TR/TE=10000/14ms, FOV=32×32 mm3, 85×85 matrix size, 1mm slice thickness with 1mm gap).
Area of acquisition	whole brain was used as area of acquisition

Diffusion MRI ☒ Used ☐ Not used

Parameters: 3 directions and 6 b values (0, 50, 100, 250, 500, 1000 s/mm2), no cardiac gaiting

Preprocessing

Preprocessing software	Matlab 2019b(MathWorks, Natick, MA, USA) for brain masking, Statistical Parametric Mapping (SPM12) for co-registration and normalization, motion correction. Segmentation of ischemic lesion to core, penumbra and edema was performed in Matlab. Tissue was compartmentalized using in house thresholds set for two parameters: (1) T2 signal change and CBF data sets; and (2) ADC and CBF data sets for PI/ADC mismatch. Color-coded images were derived based on T2 signal change and CBF values, or ADC and CBF values enabling analysis of changes in voxel distribution across ischemic core, penumbra, and edema. hemispheric volumes were determined on T2-weighted images. The hemispheres were traced manually on each slice. The position of the midline was determined with the use of the following neuroanatomic landmarks: falx cerebri, corpus

pineale, fissura longitudinalis, infundibulum, aqueductus cerebri, and third ventricle.

Normalization: Non linear normalization was used with parameters as follow: control point spacing: 1.5, smoothness: 0.01, number of levels: 3, resolution: 1.0

Normalization template: Allen Mouse brain common coordinate framework (CCFv3) template was used for normalization/transformation

Noise and artifact removal:

Volume censoring:

Statistical modeling & inference

Model type and settings:

Effect(s) tested: Data are presented as mean ± SD. Comparison of lesion evolution, and volumetric differences, T2, ADC and CBF in ischemic core, penumbra and edema across two groups were analyzed using Student's paired t-test.

Specify type of analysis: ☐ Whole brain ☒ ROI-based ☐ Both

Anatomical location(s): ROI is defined based on compartmentalization files and contralateral ROI was defined manually.

Statistic type for inference (See Eklund et al. 2016): all data were voxel based analyzed

Correction: *Describe the type of correction and how it is obtained for multiple comparisons (e.g. FWE, FDR, permutation or Monte Carlo).*

Models & analysis

n/a	Involved in the study
☒	☐ Functional and/or effective connectivity
☒	☐ Graph analysis
☒	☐ Multivariate modeling or predictive analysis